JOURNAL OF PETROLOGY | VOLUME 49 | NUMBER 8 | PAGES 1515–1547 | 2008 | doi:10.1093/petrology/egn036

The Roles of Fractional Crystallization, Magma Mixing, Crystal Mush Remobilization and Volatile–Melt Interactions in the Genesis of a Young Basalt–Peralkaline Rhyolite Suite, the Greater Olkaria Volcanic Complex, Kenya Rift Valley

R. MACDONALD[1,2]*, H. E. BELKIN[3], J. G. FITTON[4], N. W. ROGERS[5], K. NEJBERT[2], A. G. TINDLE[5] AND A. S. MARSHALL[1]

[1]ENVIRONMENT CENTRE, LANCASTER UNIVERSITY, LANCASTER LA1 4YQ, UK

[2]INSTITUTE OF GEOCHEMISTRY, MINERALOGY AND PETROLOGY, UNIVERSITY OF WARSAW, AL. ŻWIRKI i WIGURY 93, 02-089 WARSAW, POLAND

[3]US GEOLOGICAL SURVEY, 956 NATIONAL CENTER, RESTON, VA 20192, USA

[4]SCHOOL OF GEOSCIENCES, UNIVERSITY OF EDINBURGH, WEST MAINS ROAD, EDINBURGH EH9 3JW, UK

[5]DEPARTMENT OF EARTH SCIENCES, CESPAR, THE OPEN UNIVERSITY, WALTON HALL, MILTON KEYNES MK7 6AA, UK

RECEIVED MARCH 13, 2008; ACCEPTED JULY 2, 2008
ADVANCE ACCESS PUBLICATION JULY 24, 2008

The Greater Olkaria Volcanic Complex is a young (≤20 ka) multi-centred lava and dome field dominated by the eruption of peralkaline rhyolites. Basaltic and trachytic magmas have been erupted peripherally to the complex and also form, with mugearites and benmoreites, an extensive suite of magmatic inclusions in the rhyolites. The eruptive rocks commonly represent mixed magmas and the magmatic inclusions are themselves two-, three- or four-component mixes. All rock types may carry xenocrysts of alkali feldspar, and less commonly plagioclase, derived from magma mixing and by remobilization of crystal mushes and/or plutonic rocks. Xenoliths in the range gabbro–syenite are common in the lavas and magmatic inclusions, the more salic varieties sometimes containing silicic glass representing partial melts and ranging in composition from anorthite ± corundum- *to* acmite-*normative. The peralkaline varieties are broadly similar, in major element terms, to the eruptive peralkaline rhyolites. The basalt–trachyte suite formed by a combination of fractional crystallization, magma mixing and resorption of earlier-formed crystals. Matrix glass in metaluminous trachytes has a peralkaline rhyolitic composition, indicating that the eruptive rhyolites may have formed by fractional crystallization of trachyte. Anomalous trace element enrichments (e.g. ~2000 ppm Y in a benmoreite) and negative Ce anomalies may have resulted from various Na- and K-enriched fluids evolving from melts of intermediate composition and either being lost from the system or enriched in other parts of the reservoirs. A small group of* nepheline-*normative, usually peralkaline, magmatic inclusions was formed by fluid transfer between peralkaline rhyolitic and benmoreitic magmas. The plumbing system of the complex consists of several independent reservoirs and conduits, repeatedly recharged by batches of mafic magma, with ubiquitous magma mixing.*

KEY WORDS: *alkali basalt; geochemistry; magma mixing; trace element*

*Corresponding author. E-mail: r.macdonald@lancaster.ac.uk

INTRODUCTION

Many recent studies have demonstrated the complexity of silicic magma chambers, a complexity related, *inter alia*, to magma composition, the pressure–temperature conditions of formation and differentiation, the local tectonics and variable residence times within the upper crust. In addition to crystal fractionation, combined assimilation–fractional crystallization and magma mixing, many systems have evolved in part by the remobilization of crystal mushes and/or partly to completely solidified plutonic bodies that may or may not be cognate with their eruptive hosts (Nakada *et al.*, 1994; Wolff & Gardner, 1995; Burt *et al.*, 1998; Bachmann *et al.*, 2002; Bachmann & Bergantz, 2003, 2004, 2006; Tamura *et al.*, 2003; Smith *et al.*, 2004, 2005; Bacon & Lowenstern, 2005; Charlier *et al.*, 2005; Reubi & Nicholls, 2005). The complexity of the interplay between these parameters means that, in detail, every silicic system evolves in a unique way.

The majority of recent studies have focused on metaluminous systems, in both continental and subduction-related settings. None has attempted to place the evolution of a young peralkaline rhyolite system into a time–composition framework, although the differences in bulk composition, with consequent effects on phase equilibria, density, viscosity and volatile behaviour, might be expected to generate evolutionary histories different from the metaluminous cases. Furthermore, most studies of silicic systems have focused on relatively large, commonly caldera-forming, centres. In this paper, we report on the Greater Olkaria Volcanic Complex (GOVC; Fig. 1), a young peralkaline rhyolite dome and lava field in the south–central Kenya rift valley that has been marked over the past ~20 kyr by the development of at least 80 small centres from which ~15 km^3 of magma have been erupted in hundreds of eruptions. The eruptive rate can be contrasted with, for example, the highly productive Okataina centre in New Zealand, where 80 km^3 of rhyolite magma were erupted in nine episodes during the last 26 kyr (Nairn *et al.*, 2004).

An additional issue concerns the origin of peralkaline rhyolite magmas and the long-standing debate as to whether silicic magmas form by extended fractional crystallization of mafic parents or by crustal anatexis. Previous studies of the GOVC used trace element and isotopic evidence to suggest that the rhyolites formed by volatile-induced melting of heterogeneous crustal rocks (Davies & Macdonald, 1987; Macdonald *et al.*, 1987; Black *et al.*, 1997; Heumann & Davies, 2002). This left unexplained several geochemical problems, including the difficulty in generating by anatexis the very strong depletion in Ba and Sr in even the least evolved rhyolites (Heumann & Davies, 2002).

In this paper, we address the complex temporal, structural and magmatic evolution of the GOVC. We show that trachyte and rhyolite magmas formed by a combination of fractional crystallization of basalts, ubiquitous magma mixing, assimilation of earlier crystal mushes and/or plutonic material, and interactions between melts and volatile phases. Marshall *et al.* (in prep.) have addressed the further histories of the rhyolite magmas and their significance for the development of the higher structural levels of the GOVC.

The specific aims of this paper are:

(1) to provide mineral chemical and geochemical data on the basalt and trachyte eruptive rocks and on the magmatic inclusions in the peralkaline rhyolites;
(2) to determine the roles of fractional crystallization, magma mixing and remobilization of pre-existing solid material in the evolution of the basalt–trachyte suite;
(3) to re-examine the petrogenesis of the peralkaline rhyolitic magmas;
(4) to place constraints on models of the GOVC plumbing system.

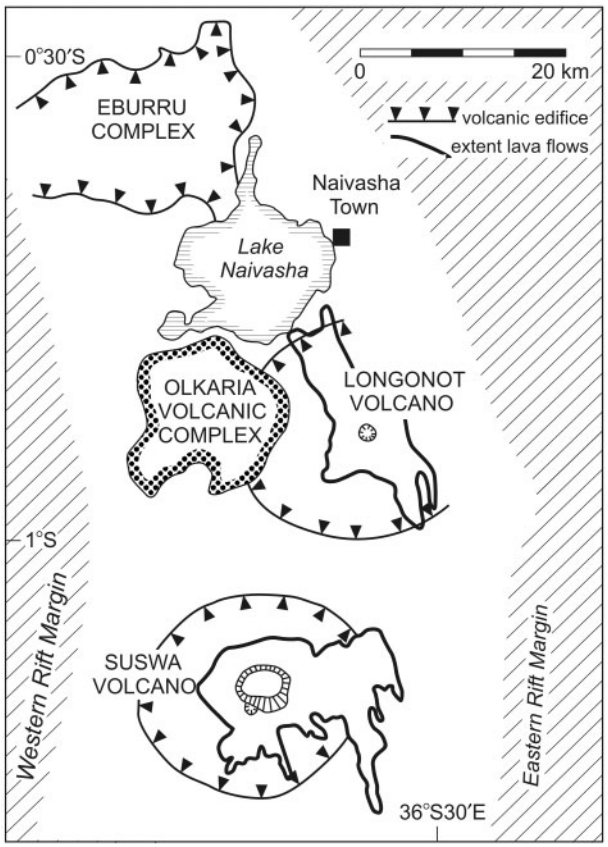

Fig. 1. Locality map of the Greater Olkaria Volcanic Complex (Olkaria), and the neighbouring centres on the Kenya Dome (Eburru, Longonot and Suswa). From Heumann & Davies (2002).

GEOLOGICAL EVOLUTION OF THE GOVC

The GOVC is part of the central Kenya peralkaline province (CKPP; Macdonald & Scaillet, 2006), which coincides with an area of crustal upwarping known as the Kenya Dome. Crustal thickness beneath the Dome is 30–35 km (Mechie *et al.*, 1997). The age of initiation of the GOVC is poorly constrained but on the basis of its relationships to the age of highstands in the local lakes, Clarke *et al.* (1990) placed it in the period 22–20 ka BP. They recognized six stages in the evolution of the complex (Fig. 2). Stage 1 was the formation of a dominantly trachytic lava and pumice pile, represented by the Olkaria Trachyte Formation (Ot) and the Maiella Pumice Formation (Mp). The pumices (not shown in Fig. 2) are widespread to the west of the complex and are thought to have been erupted from vents within it. The trachyte lavas are exposed mainly in gullies and ridges in the SW part of the complex (Fig. 2). Using evidence of (1) a well-developed ring structure, (2) the presence of a ring of rhyolite domes, (3) intra-ring volcaniclastic sedimentation, (4) apparent resurgent activity within the ring structure and (5) the distribution of fumaroles, Clarke *et al.* (1990) argued that trachyte eruption was followed (stage 2) by caldera collapse, leaving a depression 11 km × 7·5 km across. Collapse was accompanied by eruption of welded pyroclastic rocks of the Ol Njorowa Pantellerite Formation (O^1), now exposed only in the deepest parts of the Ol Njorowa Gorge (Fig. 2).

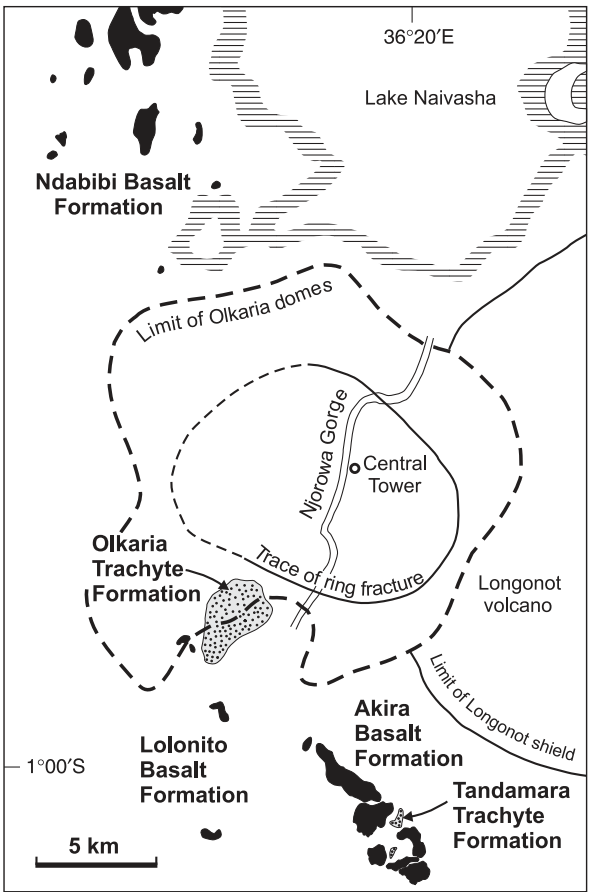

Fig. 2. General geological features of the Greater Olkaria Volcanic Complex, including peripheral basalt and trachyte formations. Based on maps of Clarke *et al.* (1990).

The earliest phase (stage 3) of post-caldera magmatism, the Lower Comendite Member of the Olkaria Comendite Formation, is represented by rhyolite lavas (O^2) and pyroclastics (Op^2), dated by ^{14}C at >9150 ± 110 BP. Stage 4, the Middle Comendite Member, was a period of ring dome formation (O^3) and eruption of thick surge deposits (Op^3). ^{14}C dates bracket its age as between 9150 ± 110 and 3280 ± 120 BP. This was followed (stage 5) by a resurgence of the caldera floor and the formation of short, thick flows, the Upper Comendite Member (O^4). The sixth stage saw the eruption of very thick flows of comendite from a north–south fissure system (O^5), the youngest flow having yielded a ^{14}C date of 180 ± 50 BP (Clarke *et al.*, 1990).

Mafic eruptive rocks occur both north and south of the dome field (Fig. 2). To the south, the Lolonito Basalt Formation (Ba^1) forms a string of small outcrops and comprises flows and pyroclastic cones with eruption ages of <0·45 Ma. The Formation may represent an early phase of the generally younger Akira Basalt Formation (Ba^2), which consists of lavas and scoria and spatter cones (Clarke *et al.*, 1990). The youngest cone is unvegetated and ungullied and may be only a few hundred years old. The formation is geographically associated with, and of the same general age as, the Tandamara Trachyte Formation (Tt), composed of welded scoriaceous lapilli and blocks and some lavas (or rheomorphic ignimbrites).

To the north of the dome field, mafic volcanism accompanied rhyolite emplacement on the Ndabibi plains, an 11 km wide, low-lying area between the GOVC and the Eburru Volcanic Complex (Fig. 2). Faulted lavas and pyroclastic cones of pre-caldera age comprise the Ndabibi Basalt Formation (Bn; Clarke *et al.*, 1990). Younger units include surtseyan tuff cones (kBt) with laterally equivalent fall tuffs (kBtm) and transitional surtseyan–strombolian ash cones (Bt). Judging from their degree of dissection, the latter units are broadly coeval with the post-caldera rhyolites (i.e. with ages of <20 ka BP).

Magmatic inclusions, ranging in size mainly from a few millimetres to 10 cm, but rarely up to ~40 cm, occur in rhyolites from all stages of post-caldera activity. They are most easily studied in faulted and/or eroded outcrops, particularly in the Ol Njorowa erosion channel. Where present, they usually make up <1% of the outcrop but rarely can be 5–10%. Magmatic inclusions also occur in composite intrusions. For example, the 50 m high Central Tower plug of O^4 age (Fig. 2) has an ~20 cm thick skin of trachyte, which was still semi-molten when intruded by

a core of comendite containing magmatic inclusions ranging in bulk composition from mugearite to benmoreite.

Two kinds of inclusion are broadly distinguishable in the field: a dark, sparsely porphyritic, more mafic variety, and purple–brown, more felsic types. The dark inclusions tend to be small (from <1 mm to ~10 cm), vary in form from sub-rounded to lensoid, have irregular, crenulated margins and low porosities (≤3%). Rare, highly vesiculated (50–60%) inclusions vary in shape but invariably have crenulated or streaky margins. Some inclusions have trails of mafic material incorporated in the comendite host, and patches and re-entrants of vesicular rhyolite occur within the inclusions. Some have pillow-like forms, sometimes with crenulate and/or chilled margins, and with inter-pillow spaces filled by rhyolite. Chilled margins are not always present, perhaps because many inclusions were small enough to chill *en masse*. Other samples show mingled zones and/or zones of vesiculation at the contacts between inclusion and host. The lighter-coloured inclusions are generally larger, up to ~40 cm, and sub-rounded to slightly elongate. The margins are crenulate but less irregularly shaped than in the dark inclusions.

The textural evidence indicates that the inclusions were incorporated into the host rhyolites in a dominantly liquid state (Bacon & Metz, 1984). Swirling of comendites and inclusions suggest mixing in eruptive conduits. More detailed textural evidence (below) shows that the inclusions themselves are very commonly mixed magma rocks.

The distribution of surface outcrops of the basalts and rhyolites indicates that the GOVC dome field displays a shadow zone, where mafic magma is prevented by its density from penetrating the overlying silicic magma, except as components of mixed rocks. The question arises as to what constitutes the Olkaria magmatic system, particularly as the Eburru Volcanic Complex and the Longonot caldera volcano lie immediately to the north and east, respectively, of the GOVC (Fig. 1). We include in the system the Ndabibi basalts, because basalts and comendites have co-erupted and mixed there, and the Akira basalts and Tandamara trachytes, because geochemically they are closely similar to the Ndabibi basalts and Olkaria trachytes.

SAMPLING STRATEGY AND ANALYTICAL METHODS

Our sampling covered, with the exception of the Maiella Pumice, the major units described above; namely, the Olkaria and Tandamara Trachyte Formations, the Lolonito, Akira and Ndabibi Basalt Formations, selected samples from the Olkaria Comendite Formation, and magmatic inclusions in the post-caldera comendites. The four available analyses of Maiella Pumice (Clarke *et al.*, 1990; our unpublished data) comprise a *ne*-normative trachyte, a *q*-normative trachyte, and two peralkaline rhyolites. Clearly a detailed petrological study of the formation, tied to attempts to identify the source vents, is necessary to assess its role in the development of the GOVC. Modal analyses of representative samples are given in Table 1.

The first record of magmatic inclusions at Olkaria was by Bone (1987) and we have used some samples collected by him (prefixed BB). Sample localities and stratigraphic units are given in the Appendix. The great majority come from O^4 but this is mainly due to increased visibility resulting from the stripping-off of flow and dyke carapaces during the formation of the Ol Njorowa overflow channel (Fig. 2). In selecting inclusions for detailed study, we tended to use only larger samples, showing insignificant macroscopic interaction with the host rock. However, in some cases the host material proved to have infiltrated deep into the inclusion. With some smaller samples (e.g. SMN111), we were unable to make both a powder and a thin section; rocks where petrographic information is missing are noted in the Appendix. In some previous publications (e.g. Davies & Macdonald, 1987; Macdonald *et al.*, 2001), Olkaria sample numbers had no prefix. Here, we prefix those rocks BL, to avoid possible confusion with those prefixed with BB or SMN.

Electron microprobe analysis (EMPA) of phenocryst and xenocryst phases in 18 samples, selected to cover the range of petrographic features in the suite, was carried out at the US Geological Survey, Reston, VA, and EMPA of a further set of phenocrysts, xenocrysts and glasses was carried out in the Department of Earth Sciences, The Open University. Details of the techniques employed in both laboratories are given in Supplementary Appendix 1 (available for downloading from the *Journal of Petrology* web site, at http://petrology.oxfordjournals.org). Representative analyses of phenocryst phases are given in Tables 2–6. The full dataset, including structural formulae and details of the analytical laboratory, is available as supplementary tables on the *Journal of Petrology* web site; these tables are referred to subsequently as ST1–8. Eighteen analyses of trace element abundances (Table 3; ST2) were made using laser ablation-inductively coupled plasma-mass spectrometry (LA-ICP-MS) at the Open University, using techniques outlined in Supplementary Appendix 1.

Major element compositions of 59 samples were determined by X-ray fluorescence (XRF) on fused discs at Lancaster University. Results for standard AGV1 are given in ST7. Representative analyses are given in Table 7 and the full dataset in ST7. Wet-chemical analyses of a further three samples were taken from Bliss (1979). For comparability with published studies, trace elements were determined on pressed powders of all rocks at the University of Edinburgh, using techniques outlined by Fitton *et al.* (1998). We also used in this study major element analyses of seven mafic rocks from Olkaria previously reported by Davies & Macdonald (1987) but with trace

elements redetermined for consistency at Edinburgh, and data for seven rocks from Macdonald *et al.* (2001) because they had recently been analysed in the Edinburgh laboratory. We have also used major and trace element data for 14 GOVC basalts and trachytes from the British Geological Survey (BGS) study by Clarke *et al.* (1990); locality details are given in Supplementary Appendix 2. No sample from their collection was available for re-analysis to check for analytical consistency. However, the datasets show no systematic differences on any chemical plot and we have assumed that they are compatible. Apart from generalized descriptions, no petrographic data were available for the Clarke *et al.* (1990) rocks. Twenty samples were analysed for trace elements (Table 8) using the ICP-MS facility at the Open University and the methods described by Rogers *et al.* (2006).

PETROGRAPHY

Phenocryst assemblages are given in the Appendix and modal analyses of 21 representative rocks in Table 1. We divide the rocks into three groups. Lacking petrographic information for the BGS samples, we have assigned them to groups on the basis of their chemical composition

Table 1: Modal analyses (vesicle-free) of Olkaria rocks

	MC	Phenocrysts									Xenocrysts		Group
		plag	oliv	cpx	oxide	alk. feld.	qtz	apat	chev	zirc	alk. feld.	plag	
Olkaria Trachyte Formation													
SMN179	–	–	+	0·7	+	31·2	–	+	–	+	+	–	1
SMN180	–	–	0·2	0·4	0·3	10·7	–	+	–	–	+	–	1
SMN199	–	–	0·1	2·1	0·1	24·2	–	+	+	+	–	–	1
BB85.293	–	–	+	+	0·5	28·8	2·2	–	–	–	–	–	
Lolonito Basalt Formation													
SMN164i	1	0·9	0·05	0·3	0·2	–	–	–	–	–	1·1	+	1
Ndabibi Basalt Formation													
BL64	–	2·0	0·1	0·2	–	–	–	–	–	–	–	–	1
BL25	–	16·6	1·1	4·5	–	–	–	–	–	–	–	–	1
BL124	–	4·2	0·3	0·7	–	–	–	–	–	–	1·3	+	1
BL146a	1	10·3	1·3	3·3	–	–	–	–	–	–	–	–	1
BL158a	1	16·2	1·1	3·5	0·2	–	–	–	–	–	–	–	1
BL120c	–	3·4	0·2	0·8	–	–	–	–	–	–	3·9	–	2
Akira Basalt Formation													
BB85.42	–	1·2	0·05	0·8	–	–	–	–	–	–	0·45	–	2
Tandamara Trachyte Formation													
BB85.19	–	–	0·2	0·8	0·5	19·8	–	+	–	+?	–	–	1
BB85.18	–	–	+	0·4	0·4	24·8	–	+	+	+	–	–	1
Olkaria Comendite Formation													
BB85.268	1	–	+	0·4	0·3	0·6	–	+	–	–	1·4	–	1
SMN105	1	–	0·1	+	–	4·3	0·3	+	+	–	+	*	
SMN168	1	–	0·2	0·6	0·4	6·4	+	+	+	–	–	–	1
BL574	1	2·6	0·2	0·4	–	–	–	–	–	–	6·1	5·9	
Magmatic inclusions													
BB85.278	–	0·3	+	0·2	0·1	–	–	–	–	–	2·3	+*	1
BB85.40	–	–	0·4	1·2	0·2	4·5	–	+	–	–	8·8	+	1
BB85.26	1	–	+	0·5	0·1	–	–	–	–	–	5	–	1

Group indicates the petrographic/geochemical groups (see text). +, present but <0·1%. MC, mix component from Appendix.
*Contains cpx xenocrysts.

(see below). A main suite (Group 1) ranges in bulk composition from basalt through hawaiite, mugearite, benmoreite and trachyte to rhyolite. The group is represented by extrusive rocks and magmatic inclusions and includes various kinds of mixed magma rocks. Group 2 comprises rocks with bulk compositions in the hawaiite–benmoreite range, but compositionally different from Group 1, formed by the mixing of basaltic and trachytic or rhyolitic magmas. This group is dominated by extrusive rocks but includes a few magmatic inclusions. Five silica-undersaturated magmatic inclusions constitute Group 3. All three groups contain an extensive suite of feldspar xenocrysts and gabbroic to syenitic xenoliths in various states of disaggregation.

Basalts and hawaiites

The mafic rocks (Lolonito and Ndabibi Basalt Formations, mafic components of mixed rocks) are plagioclase-phyric, with subordinate olivine and clinopyroxene phenocrysts (Table 1; Appendix). There are two petrographic types, finely (more sparsely) and coarsely porphyritic, which do not differ significantly in chemical composition. The two types occasionally occur in the same flow. The less-phyric rocks (e.g. BL64) contain <5% plagioclase phenocrysts ≤2 mm long; these tend to be euhedral, although some internal resorption is common. Plagioclase crystals in more coarsely porphyritic varieties (e.g. BL25, BL158a) typically form 10–20% modally, and are elongate laths or blocky crystals up to 5 mm long. They are weakly zoned and some show poorly developed sieved interiors with partially resorbed rims. Olivine and clinopyroxene phenocrysts in both varieties tend to be small (<1 mm) and subhedral to euhedral. Glomeroporphyritic clusters of all three phenocryst phases are very common.

Mugearites and benmoreites

Phenocrysts (plagioclase + clinopyroxene + FeTi-oxides ± olivine) in the mugearites and benmoreites tend to be smaller and less abundant than in the basaltic rocks; some rocks are aphyric (e.g. BB84.24, BB84.39; Appendix). The plagioclase most commonly forms laths up to 0·5 mm long, some showing swallowtail terminations and, occasionally, hollow cores; these textures indicate rapid growth from the magma (Lofgren, 1980). Olivines are scarce, colourless, small (<0·15 mm) and usually associated with clinopyroxene. The clinopyroxene phenocrysts are typically small (≤0·2 mm), colourless and slightly rounded; they tend to occur in clusters, sometimes with plagioclase. The FeTi-oxides are equant, small (≤0·2 mm) and also tend to cluster together.

Trachytes

Where fresh, the trachytes are massive and grey but some are microvesicular and some have a brownish colour as a result of oxidation. They contain up to 32% phenocrysts (Table 1), the assemblage being alkali feldspar + olivine + clinopyroxene + FeTi-oxide + apatite ± zircon ± chevkinite ± sulphide. The dominant phase is blocky alkali feldspar, up to 7 mm across, usually retaining euhedral or subhedral form but almost invariably strongly resorbed internally. Many crystals are simply zoned. Some rocks (e.g. SMN180) contain a generation of almost totally resorbed feldspars. Olivine phenocrysts are most commonly present as colourless prisms, up to 1·5 mm long, showing varying degrees of resorption. The clinopyroxene crystals are grey–green, small (<1·5 mm) and fairly euhedral, although normally showing incipient resorption. FeTi-oxides are usually equant in form and <1 mm, rarely up to 2 mm, in size; they can be discrete or included in clinopyroxene or alkali feldspar. Apatite microphenocrysts sometimes occur as discrete crystals but more commonly are associated with, or included in, clinopyroxene, FeTi-oxide, olivine or alkali feldspar. Crystals are prismatic, up to 300 μm long, frequently show simple or oscillatory zonation (with zones ~10 μm across), and may have a central hollow. Zircon and chevkinite microphenocrysts are relatively scarce, typically only a few grains per thin section, and occur either as discrete crystals or in association with alkali feldspar, clinopyroxene and FeTi-oxide. Crystals are elongated, up to 350 μm long, and either euhedral or with a slightly rounded form.

Mixed magma rocks

We distinguish two types of mixed magma rocks; mingled, where two or more melt components have not completely blended, and hybridized, where the mixing process has produced a well-blended magma, the mixing stage being recorded mainly in disequilibrium phenocryst assemblages. Mixed magma rocks are found in all three groups as defined above. Mixing takes two forms in Group 1: mixing of basaltic magmas and mixing of mugearites, benmoreites, trachytes and rhyolites in various proportions. The dominant expression of basalt–basalt mixing is a streaky admixture of melts of slightly different composition and/or texture. For example, the matrix in BB85.250 has two intimately intermixed components: one is slightly coarser and carries plagioclase microphenocrysts; the other is finer-grained, lacks plagioclase microphenocrysts, is rather more clinopyroxene-rich and tends to form spheres in the coarser component. A less common form of basalt–basalt mixing is exemplified in BL146a (Fig. 3a), where rounded inclusions of a titanaugite-bearing, oxide-rich basalt, up to 8 mm across and forming 12% modally, are embedded in a more typical olivine basalt. A high Ti content in pyroxene typically indicates high rates of crystallization (Feeley & Dungan, 1996).

The second type of mixing in Group 1, found also in Group 3, occurs in the magmatic inclusions. They contain one or more components in the mugearite–rhyolite compositional range in various degrees of mingling and hybridization. Some representative examples are shown in Fig. 3.

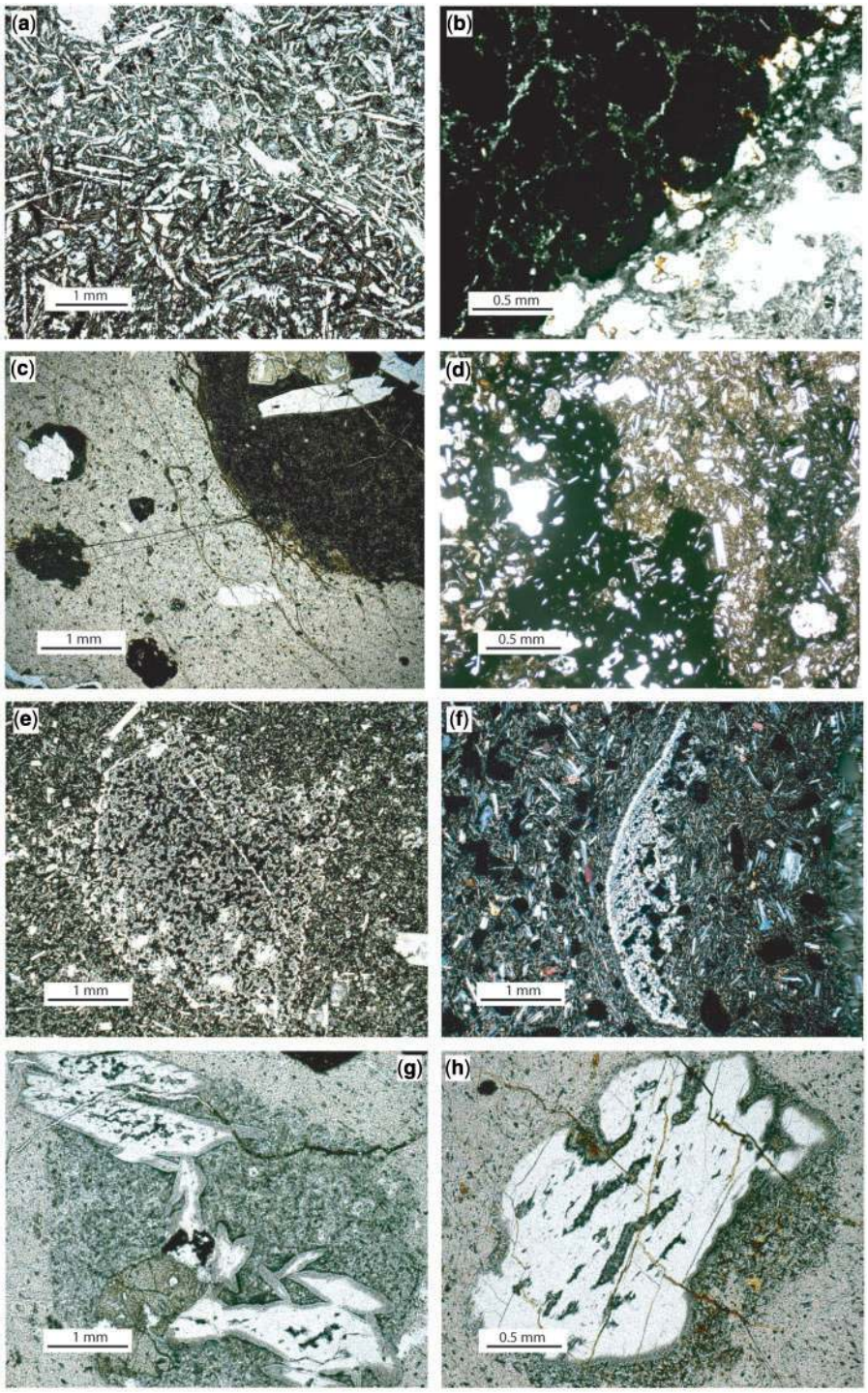

Fig. 3. Selected examples of magma mixing relationships, xenocrysts and xenoliths in GOVC rocks. (a) Contact of a 1 cm spherical inclusion of basalt (lower) against the host vesicular basalt (upper). (Note acicular mafic minerals in the inclusion.) Sample BL146a. (b) Mafic magma chilled to micropillow forms in comendite host (to right). Comendite fills the interstices between pillows. Both magmas have vesiculated. SMN75. (c) Mafic inclusions (dark) with crenulated margins in comendite (light brown). Largest inclusion contains a disaggregating gabbro xenolith; inclusion at top left contains partially resorbed alkali feldspar xenocryst. SMN105. (d) Mafic magma sending fingers into brown salic host. Grey material to left and right may be third magmatic component. SMN103. (e) Heavily resorbed alkali feldspar xenocryst in mugearitic host. (Note discontinuous white rim to the feldspar.) BL120c. (f) Crescent-shaped remnant of resorbed alkali feldspar xenocryst (with white rim) in basalt host. BL226a. (g) Disaggregating syenite xenolith in magmatic inclusion of intermediate composition in comendite host. Partially resorbed feldspars have dendritic rims. Clinopyroxene (green; bottom left) is partially resorbed. SMN105. (h) Partially resorbed alkali feldspar xenocryst, with discontinuous dendritic rim (e.g. bottom of crystal), with jacket of intermediate-composition melt in comendite host. (Note mixing of inclusion and host along right-hand contact.) SMN105.

The mafic material has commonly chilled to pillows, 0·5–1 mm across; in some cases, the comendite host has filled the interstices between pillows and is often fluorite- and riebeckite-rich (Fig. 3b). Vesiculation of host and/or inclusion magmas at their contact is common (Fig. 3b). In Fig. 3c, the mafic magma has dispersed into rounded to crenulated blebs within the comendite host (light brown). This sample (SMN105) contains 22% of mafic inclusions but most samples have significantly smaller amounts (e.g. 3·4% in SMN168 and 1·3% in BB85.26). In some cases, as shown in Fig. 3d, the mafic magma has fingered into the salic host; the slightly greyer material on the right may be a third component or a mix of the other two. There is sometimes a zone of intermediate composition between the rhyolite host and the inclusion, formed either by physical commingling or diffusive mixing of the melts (Fig. 3g and h).

The petrographic and textural relationships in Group 1 clearly indicate that the inclusions range from single-component (unmixed) melts to, more commonly, mixtures of two, and more rarely three or four, magmatic components. In BB85.269N, for example, the components range from mugearitic to trachytic. The inclusions were then intruded into, and locally interacted with, the comendite melts. The extrusive trachytes show little evidence of mingling but it is clear from phenocryst compositions (below) that at least three flows (SMN179, SMN180, BB85.18) are hybrids.

Group 2 comprises rocks from the Ndabibi, Lolonito and Akira Basalt Formations and two magmatic inclusions (Appendix). They are mingled (BB85.38, SMN103, BB85.94, BL229, BL469, SMN158, BL136) or hybridized (BL120c, BB85.42, 860130, BB85.93, BL74, BL563a, BL574) mixtures of mafic and trachytic or rhyolitic (comendite and pantellerite) magmas. The two components normally form streaky or patchy mixtures at a scale <2 mm.

Perhaps the most notable feature of the Group 3 rocks, all magmatic inclusions, is the intimate character of the interaction between the inclusions and their rhyolitic hosts. In BB84.39 and BB85.185, the mafic component quenched into micro-spherules <1 mm in diameter, enclosed by, and sometimes veined by, salic material, often rich in fluorite and sodic amphibole. In SMN153, the mafic inclusion was breaking up in, and was veined by, the host. The two components in SMN121 are streaked out and rolled together. Mixing at the junction between inclusion and host was common.

In summary, mafic, intermediate and salic magmas have been present contemporaneously in the Olkaria system for at least the past 20 kyr and have very frequently mixed at various stages during ascent and eruption.

Xenocrysts and xenoliths

A significant proportion (59%) of the mafic–intermediate extrusive rocks and magmatic inclusions carry large (up to 6 mm) grains of alkali feldspar, and less frequently plagioclase, forming up to 9% modally (Table 1; Appendix). Such feldpars invariably have a jacket of more mafic material against the rhyolitic host (Fig. 3g and h), a feature reported for large xenocrysts of alkali feldspar in intermediate enclaves at the Gedemsa volcano in Ethiopia by Peccerillo *et al.* (2003). The feldspars are generally intensely embayed and resorbed, to the extent that they can be difficult at a cursory glance to distinguish from the host matrix (Fig. 3e). The patchy replacement of plagioclase by sanidine and the growth of calcic dendritic rims on sanidine are almost certainly a response to magma mixing (Hibbard, 1981). The growth of dendritic plagioclase has been reproduced experimentally and is highly dependent on the degree of undercooling of the mafic melt (Lofgren, 1974). Textural and compositional relationships are complex, depending, as we shall see below, on the number and proportions of mixing components.

Coarse-grained xenoliths ranging in composition from gabbro (SMN105; Fig. 3c) through syenodiorite–syenite (SMN166, BB85.40, SMN153, BB85.278) to syenite (SMN105, Fig. 3g; BB85.268) commonly form strings up to 7 mm long and have almost invariably been partially disaggregated by resorption. In some cases, the alkali feldspars show dendritic rims (Fig. 3g and h).

Glass-bearing feldspars and feldspar aggregates occur in samples SMN103, BL225a and SMN168I. In SMN103, the mugearitic host magma has infiltrated into a plagioclase crystal ($An_{32·0}Ab_{61·7}Or_{6·4}$) (Table 2) along cleavage planes and has largely replaced the inner parts of the crystal. The residual feldspar is penetrated by glass (Fig. 4). A 5 mm × 3 mm xenolith (no. 3) in BL225a comprises residual alkali feldspar crystals slightly reverse zoned from $An_{0·1}Ab_{59·2}Or_{40·7}$ to $An_{1·7}Ab_{60·9}Or_{37·4}$ (Table 2) in a matrix with two components (Fig. 5): a clear glass showing perlitic cracks, and sub-rounded areas up to 300 μm across containing vermicular quartz and platy feldspar in grey glass. There was some mingling of the two textural varieties of melt along their contacts.

Xenolith 1 in BL225a is 10 mm × 6 mm and comprises alkali feldspar ($An_{3·3–0·2}Ab_{60–64}Or_{33–40}$) in glass that is dominantly pale brown, with much less abundant, arcuate patches of deep brown glass. Xenolith 2 (6 mm × 3 mm) is similar except that the deep brown glass usually contains irregular aggregates of FeTi-oxides (Fig. 6). SMN168I carries a 5 mm long cluster of alkali feldspars that have been partially melted along their rims. The residual feldspars have the average composition $An_{0·2}Ab_{56·7}Or_{43·1}$ and there are two types of glass, one deep brown, the other pale brown to colourless and containing minute oxide filaments. Following Bachmann *et al.* (2002), we suggest that the oxide filaments were formed during incipient devitrification, rendering the surrounding glass colourless, whereas the oxide-free glass areas retained their brown colour.

Table 2: Analyses of feldspars in Olkaria rocks

	Phenocrysts											
Strat.:	Ndabibi Basalt Formation				Magmatic inclusions				Olkaria Trachyte Formation			
Sample:	BL158a		BL229		BB85.40		BB85.278		SMN179		SMN199	
Group:	1		2		1		1		1		1	
MC:	1		1		hyb		hyb		hyb		—	
	core	rim	core	rim	core	rim	core	rim	core	core	core	rim
SiO_2	45·68	47·33	51·78	51·27	56·29	55·54	58·52	56·12	63·49	63·85	66·27	65·77
Al_2O_3	33·88	33·16	29·65	29·88	26·57	27·30	25·01	26·65	21·37	21·14	18·96	19·66
Fe_2O_3*	0·50	0·61	0·67	0·71	0·78	0·79	0·34	0·64	0·18	0·20	0·20	0·18
CaO	18·13	16·80	13·47	13·92	9·49	10·25	6·56	9·16	2·64	2·62	0·34	0·99
SrO	0·10	0·06	0·09	0·12	0·14	0·16	—	—	0·05	0·07	0·04	0·00
Na_2O	1·23	1·80	3·87	3·49	5·63	4·98	6·01	6·25	6·90	6·72	5·54	6·01
K_2O	0·01	0·05	0·19	0·19	0·57	0·54	1·96	0·54	4·04	4·23	8·16	7·00
BaO	0·00	0·00	0·00	0·00	0·04	0·13	0·96	0·27	0·75	0·76	0·00	0·00
Total	99·53	99·81	99·72	99·58	99·51	99·69	99·36	99·63	99·42	99·59	99·51	99·61
An	88·8	82·8	65·0	68·1	46·6	51·5	33·3	43·4	13·3	13·2	1·7	4·9
Ab	10·9	16·0	33·9	30·8	50·0	45·3	55·0	53·6	62·6	61·4	49·9	53·8
Or	0·3	1·2	1·1	1·1	3·4	3·2	11·8	3·0	24·1	25·4	48·4	41·3

	Xenocrysts										p.m. syenites	
Strat.:	Magmatic inclusion					Olk. Com. Fm			Magmatic incl.		LBF	NBF
Sample:	BB85.40					BB85.268			SMN111		SMN103	BL225a
Group:	1					1			?		2	1
MC:	hyb					1			—		1	—
	core	dend	core	core	rim	core	rim	core	rim	dend	av.	rim
SiO_2	62·34	60·59	57·97	59·87	60·30	56·83	56·77	62·30	61·44	62·51	58·89	66·00
Al_2O_3	20·84	22·67	25·35	23·21	22·37	26·06	26·60	21·52	22·21	22·33	24·27	18·08
Fe_2O_3	0·20	1·51	0·38	0·31	0·27	0·42	0·63	0·21	0·22	0·83	0·36	1·08
CaO	1·54	4·07	7·91	5·32	4·19	8·23	9·12	3·25	3·69	5·04	6·63	0·33
SrO	0·03	0·12	0·09	0·09	0·12	—	—	0·02	0·06	0·09	—	—
Na_2O	4·65	6·10	5·90	6·09	5·65	5·29	5·41	6·02	6·00	6·84	7·05	6·63
K_2O	7·35	3·21	1·57	2·88	3·99	1·25	0·74	5·00	4·67	1·49	1·11	6·18
BaO	2·94	1·06	0·55	1·03	1·69	0·86	0·28	0·71	1·24	0·45	—	0·00
Total	99·89	99·33	99·72	98·80	98·58	98·94	99·55	99·03	99·53	99·58	98·31	98·30
An	8·2	21·5	38·9	26·9	21·9	42·7	46·0	16·2	18·4	26·3	32·0	1·7
Ab	45·0	58·3	52·2	55·7	53·4	49·6	49·5	54·2	54·0	64·4	61·7	60·9
Or	46·8	20·2	9·1	17·3	24·8	7·7	4·5	29·6	27·6	9·3	6·4	37·4

Olk. Com. Fm, Olkaria Comendite Formation; LBF, Lolonito Basalt Formation; NBF, Ndabibi Basalt Formation. MC, mix component (see Appendix). hyb, hybrid rock; dend, dendritic rim; p.m. syenites, feldspars in partially melted syenites.

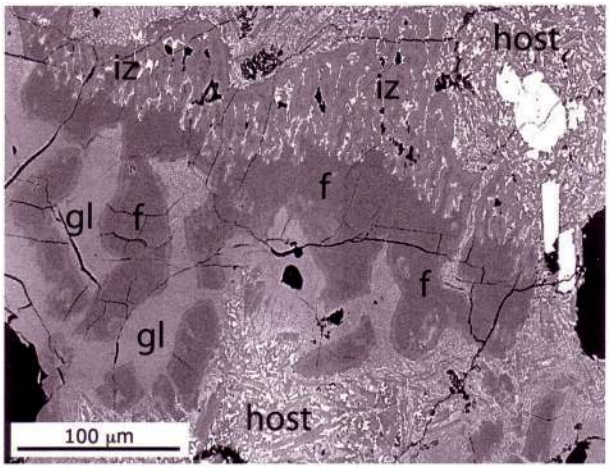

Fig. 4. BSE image of the resorption and partial melting of a plagioclase xenocryst by the host mugearitic magma in SMN103. f, feldspar; gl, glass; iz, infiltration zone.

MINERAL CHEMISTRY

Feldspars

Phenocrysts

Plagioclase phenocrysts in the mafic rocks, up to 17% modally (Table 1), form subhedral to euhedral plates up to 4 mm × 3 mm, although incipient resorption features are common. Core compositions are in the range $An_{89–38}$ (Fig. 7; Table 2; ST1a) and the extent and type of zoning (up to 8% An content) vary between rocks.

In the mugearites and benmoreites, core compositions are in the range $An_{57–30}$ and zoning is modest (An ≤8). Alkali feldspar phenocrysts in the trachytes are mainly sanidine, but many crystals have anorthoclase cores (Table 2; ST1b). In SMN180, for example, the range of core compositions is $An_{19–2}$. Both normal and reverse zoning occur, usually modest (An <4). There are several trends within the sanidine crystals; for example, the displacement of the trends for SMN180, SMN199 and SMN168 in Fig. 7a (inset) should be noted. The shift is probably related to compositional differences in the parental magmas.

Xenocrysts

Compositions are presented in ST1c. We exemplify the complexity using one rock, although we stress that all the mafic and intermediate rocks are to some degree unique in terms of their xenocryst content and composition. We have attempted to distinguish hybrid phenocryst assemblages from higher-temperature residuals by the presence of reverse zoning in the former but we note that such zoning can also be formed by reheating without mixing.

In the mixed magma rock BB85.40 (Fig. 7b), plagioclase phenocrysts ($An_{52·2}$, $An_{46·6}$), comprising euhedral laths some 80 μm × 200 μm, show modest reverse zoning (An <5). Phenocrysts of composition $An_{40–30}$, forming partly resorbed, platy crystals ~300 μm × 200 μm in size, show modest normal zoning (An <7). Xenocryst 1 is reversely zoned from $An_{8·2}$ to $An_{21·5}$. Xenocryst 2 (not shown) has darker and lighter core zones [on back-scattered electron (BSE) images] of $An_{38·7}$ and $An_{8·7}$, respectively, and

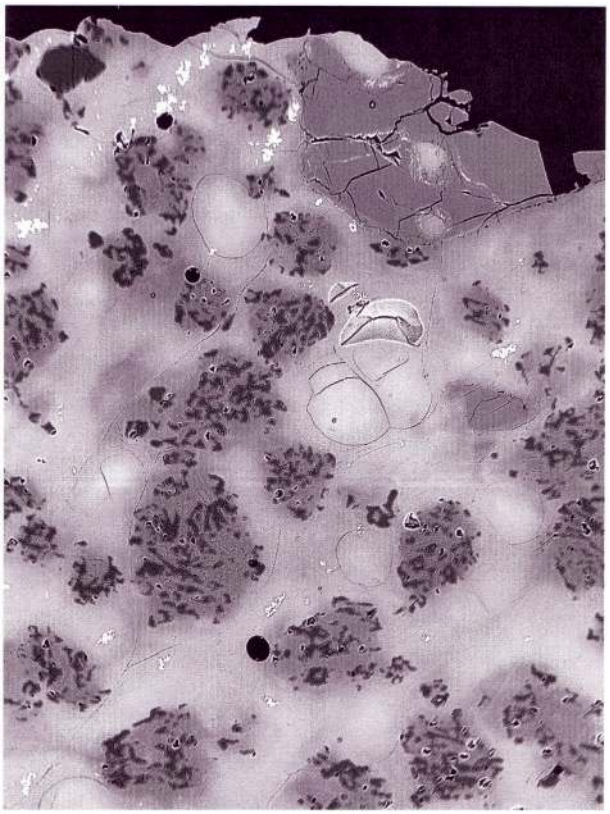

Fig. 5. Syenite(?) xenolith (residual sanidine grain at top right) has been melted to produce a pale glass (with perlitic cracks) and a darker glass containing vermicular quartz and feldspar microlites. Sample BL225a, xenolith 3. BSE image is 900 μm across.

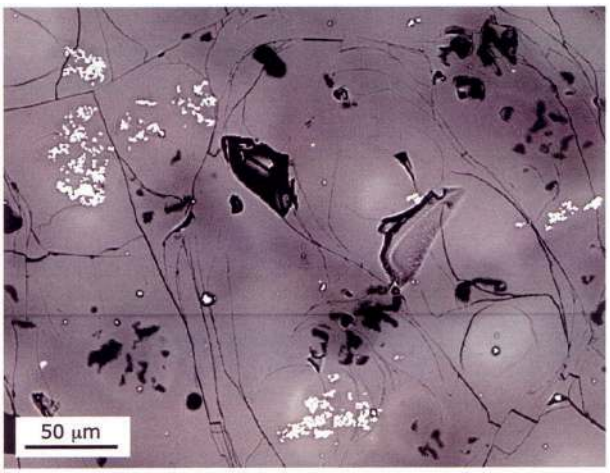

Fig. 6. BSE image of irregular aggregates of FeTi-oxides (bright) in deep brown glass areas in xenolith 2 in BL225a, interpreted as residual from partial melting.

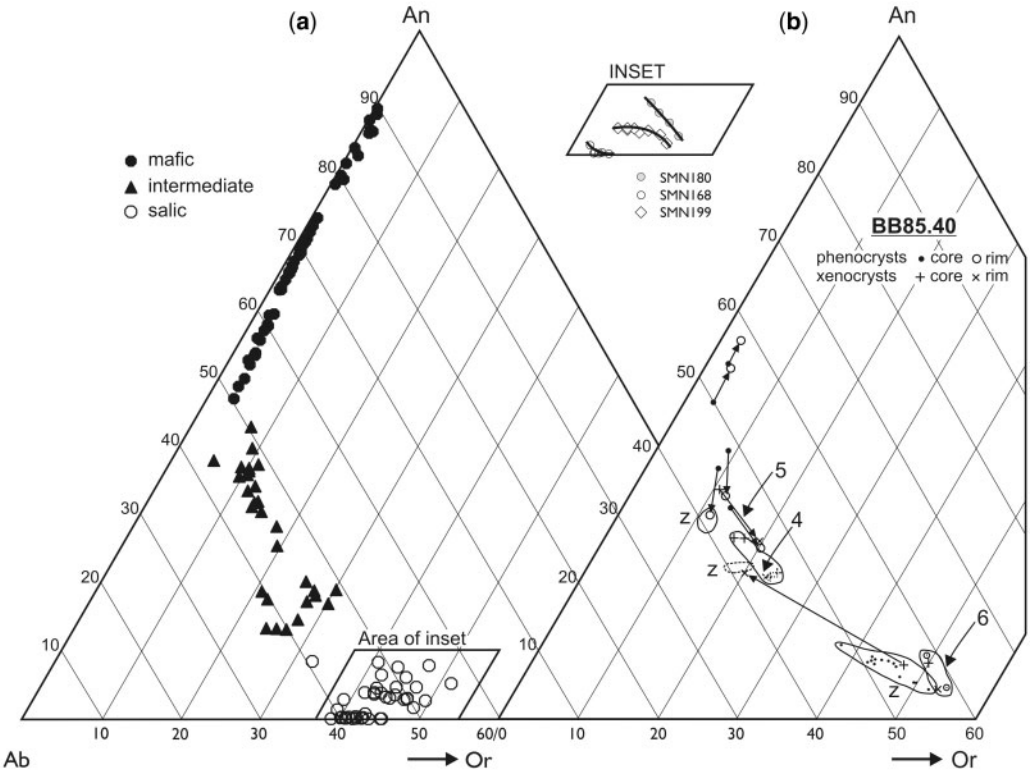

Fig. 7. (a) The compositions of feldspar phenocryst cores plotted on an An–Ab–Or diagram. Data from ST1a,b. The inset shows data for SMN180, SMN199 and SMN168, to exemplify the different trends within the sanidines in the trachytes. (b) Compositions of feldspar phenocrysts and xenocrysts in mixed magma rock BB85.40. Arrows connect crystal cores and rims. Numbers refer to the crystal numbers presented in the ST1c and as discussed in the text. Z is the 5 mm xenocryst referred to in the text.

a dendritic rim of $An_{25.7}$. Xenocrysts 4 and 6 are patchily zoned between An_{27} and An_{21} and xenocryst 5 is normally zoned from $An_{33.8}$ to An_{26}. Overall, it seems that sodic plagioclase and sanidine phenocrysts from mugearitic and trachytic magmas, respectively, were attempting to re-equilibrate to $\sim An_{25}$ after mixing, the composition in equilibrium with the new melt composition. The reverse zoning from andesine to labradorite requires a different explanation. It may have been caused by the host basalt mixing with, or being heated by, a more magnesian magma, or by loss of a volatile phase before mixing with the trachyte.

We have also made several electron microprobe analyses of a large (5 mm) crystal in BB85.40 (Z in Fig. 7b; Fig. 8), which shows significant resorption by the host magma. Although the textural relationships are complex, we distinguish an outer calcic zone ($>An_{20}$), an interior zone patchily replaced by An_8, and bright zones on the BSE image which tend to have the highest Ba contents in the crystal (BaO $\leq$5·61 wt%; Cn 11%). The substitution scheme in this crystal, and in all the xenocrysts, is $Ba + Al \leftrightarrow K + Si$.

The compositional range in this crystal covers much of the range in the phenocrysts (Fig. 7a). Our interpretation is that an alkali feldspar xenocryst was incorporated into trachyte magma and was being intensely, patchily replaced before its host was admixed with a more mafic magma (benmoreite?) and the dendritic rim was formed.

A comparable situation is found in a 4 mm crystal in SMN111 (Fig. 9): a partially resorbed, patchily replaced feldspar (An_{21-16}) has a narrow dendritic rim (An_{26}). Our interpretation is that the crystal was incorporated into a melt (the lighter zone in the image) more mafic than that from which it crystallized and a more calcic, dendritic rim was formed (Hibbard, 1981), followed by intense resorption. Before resorption was completed, the crystal plus surrounding melt were mixed into the host rhyolite (darker zone).

Anhedral, partially resorbed plagioclase xenocrysts, patchily zoned and up to 2 mm across, have been found in eight rocks. They occur singly or in glomerophyric clusters, often involving alkali feldspar. We have analyses from two rocks, both indicating reverse zoning, in BB85.268 from $An_{42.7}$ to $An_{46.1}$ and in BB85.278 from $An_{35.3}$ to $An_{43.3}$.

The question remains as to the source of the large xenocrysts. In many cases, the alkali feldspars were derived from a trachytic magma; their size and composition match the phenocrysts in the trachytes. However, the plagioclase and ternary feldspars, too calcic to have

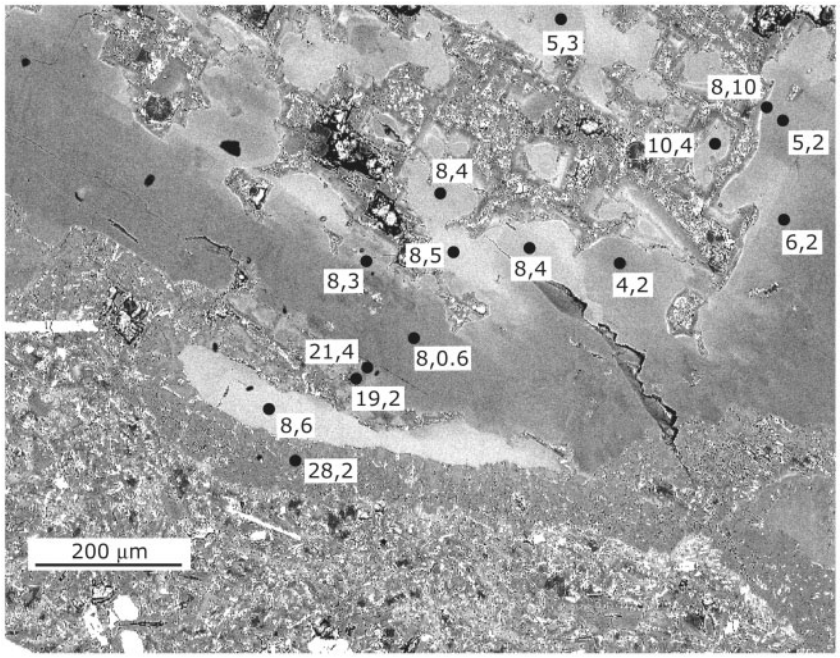

Fig. 8. BSE image of an alkali feldspar xenocryst in BB85.40. The dots refer to points analysed by electron microprobe; the numbers are the An and Cn (mol %) contents at each point. Data from ST1c.

crystallized from trachyte, may have been part of coarse-grained, solidified rocks, such as the syenodiorites and syenites found in BB85.278, or from crystal mushes. Such recycled crystals have been termed 'antecrysts' by W. Hildreth (see Bacon & Lowenstern, 2005).

Trace elements in feldspars

Barium and Sr contents of feldspar phenocrysts and xenocrysts have been determined by EMPA (Table 2; ST1). In addition, Ba, Cs, Ga, Li, Pb, Rb, Sr and the rare earth elements (REE) have been determined by LA-ICP-MS in feldspar phenocrysts from the mafic portion of a mixed rock, a trachyte, a mixed dyke rock and a magmatic inclusion (Table 3; ST2).

Barium contents in the feldspar phenocrysts and xenocrysts show a peaked distribution against An content. In the more calcic (An >30) and least calcic (An <5) feldpars, Ba is generally low (<0.10 a.p.f.u.). Between An_{30} and An_5, and peaking at An_{10}, many are notably Ba-rich, the maxima being 5·61 and 8·78 wt% BaO determined by EMPA and LA-ICP-MS, respectively, in BB85.40 (Tables 2 and 3). Barium contents thus peaked in trachytic melts somewhat less evolved than the eruptive trachytes. In contrast, all the feldspars are Sr-poor (SrO ≤0·16 wt%). Sr contents generally decrease, and Rb contents increase, with decreasing An content.

Chondrite-normalized REE patterns for feldspars are shown in Fig. 10. The plagioclase phenocryst (An_{87}) in the basalt is light REE (LREE)-enriched relative to the heavy REE (HREE), which are all below detection, and shows a positive Eu anomaly ($Eu/Eu^* = 12$). Feldspars in the mixed rocks have compositions in the range $An_{36–20}$. The REE patterns are broadly intermediate between those for the basalt and trachyte but with very large, positive Eu anomalies ($Eu/Eu^* = 183–1137$).

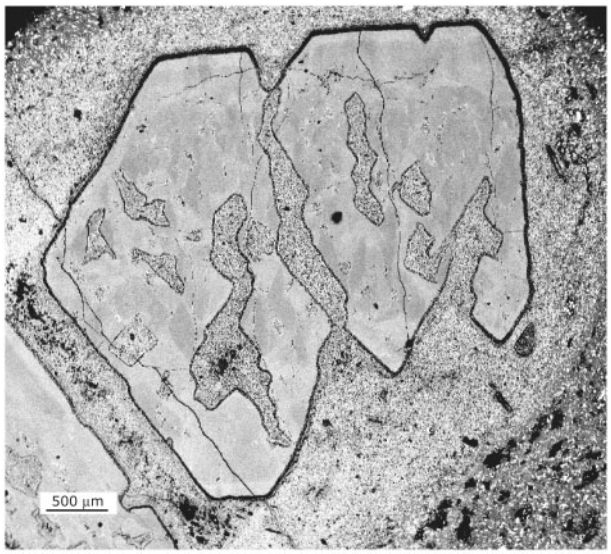

Fig. 9. BSE image of an alkali feldspar xenocryst in sample SMN111, intensely resorbed but still retaining a partially euhedral form. (Note the dark dendritic rim.) The feldspar has a jacket of mugearitic(?) composition (lighter), which is itself an inclusion in a comenditic magma (darker).

Table 3: Major (EMPA) and trace (LA-ICPMS) element analyses of feldspars in GOVC rocks

Strat. unit:	Olkaria Trach. Fm		Ndab. B.	Olkaria Com. Fm		Magmatic inclusion		
Sample:	SMN199		BL229	BB85.268		BB85.40		
Group:	1		2	1		1		
Identifier:	1-EB	6-EN	FB	1-HC	3-HD	4-HA	4-HD	Y-HI
Form:	P	P	P	P	P	P	P	P
SiO_2	64·71	64·24	45·72	61·23	57·91	60·64	60·21	58·87
Al_2O_3	19·22	19·45	32·79	21·75	24·60	22·25	22·52	23·11
Fe_2O_3	0·17	0·13	0·53	0·27	0·40	0·24	0·27	0·31
CaO	0·91	1·01	17·66	3·84	7·04	4·21	4·34	5·06
SrO	—	—	—	—	—	0·06	0·08	0·10
BaO	0·01	0·05	0·00	1·18	0·99	1·56	1·68	1·85
Na_2O	6·14	5·95	1·43	5·76	5·68	5·79	5·73	5·82
K_2O	7·03	7·27	0·03	4·16	1·68	3·93	3·74	3·18
Total	98·19	98·1	98·16	98·19	98·30	98·68	98·57	98·3
Or	41·0	42·4	0·2	25·8	10·4	24·2	23·2	19·5
Ab	54·5	52·7	12·7	54·3	53·2	54·1	54·1	54·4
An	4·5	4·9	87·1	20·0	36·4	21·7	22·7	26·1
Ba	75	656	61	—	—	19807	20115	27340
Cs	0·03	0·05	—	—	0·05	0·51	0·26	0·21
Ga	25	28	20	27	25	28	27	36
Li	5·5	6·1	4·3	3·1	2·1	5·4	6·0	7·3
Pb	5·8	7·5	0·2	3·2	3·1	2·9	3·0	2·7
Rb	73·0	69	0·13	17	27	19	18	12
Sr	15	51	901	922	1006	771	744	1877
La	10·6	15·6	1·1	6	5·3	7·3	4·8	9·5
Ce	8·2	19·3	1·7	7·0	7·9	8·1	6·3	11·4
Pr	0·38	1·0	0·19	0·58	0·66	0·77	0·44	0·94
Nd	0·70	2·8	0·67	1·7	2·1	2·5	1·2	3·2
Sm	—	0·37	0·14	0·15	0·36	0·22	0·08	0·33
Eu	0·81	2·1	0·36	28	19	23	20	27
Gd	—	0·20	0·09	0·07	0·33	0·18	0·06	0·27
Tb	—	0·04	—	0·02	0·04	0·02	0·01	0·03
Dy	—	0·20	0·03	0·05	0·20	0·12	0·05	0·11
Ho	—	0·04	—	0·01	0·03	0·04	0·01	0·03
Er	—	0·16	—	0·01	0·10	0·09	0·03	0·14
Tm	—	0·02	—	—	—	0·01	0·01	0·02
Yb	—	0·16	—	—	0·11	0·06	0·05	0·27
Lu	—	0·02	—	—	0·02	0·01	0·01	0·05
$[La/Yb]_{CN}$	—	60	—	—	35	88	69	25
Eu/Eu^*	—	20	12	600	183	382	850	295

Ndab. B., Ndabibi Basalt Formation; P, phenocryst; x, xenocryst.

Alkali feldspar in the trachyte shows a steeper decrease towards the middle REE (MREE) ($[La/Sm]_{CN} = 72$, as opposed to 5 in the basalt) but a fairly flat pattern between the MREE and HREE. The Eu anomaly is smaller than in the ternary feldspars ($Eu/Eu^* = 20$). The maximum Eu anomalies are, therefore, generally found in the more Ba-rich feldspars. REE abundances and chondrite-normalized patterns vary both within crystals (e.g. Ce from 4 to 8 ppm in crystal 1, SMN199) and between crystals in the same rock (e.g. 4–11 ppm in crystal 1 and

11–16 ppm in crystal 6, SMN199), which may have been related to element diffusion during reheating and mixing events.

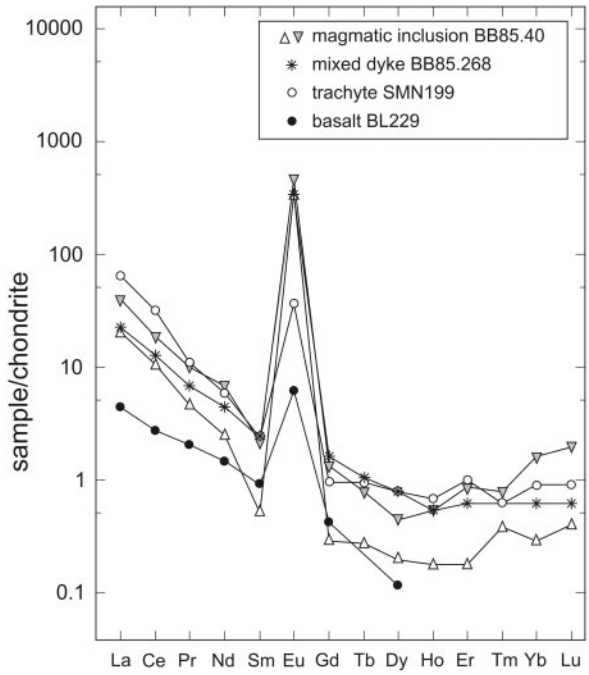

Fig. 10. Chondrite-normalized REE patterns for representative feldspar phenocrysts and xenocrysts. Normalizing factors from Sun & McDonough (1989). Data from Table 3: BL229, analysis FB; SMN199, analysis 6-EN; BB85-268, 3-HD; BB85.40, analyses 4-HD and Y-HI.

Olivine

Olivine phenocryst cores in the mafic rocks are in the range $Fo_{88–65}$ (Table 4; ST3). Zoning, where present, is normal (Fo <6). Core compositions in the mugearites are more Fe-rich ($Fo_{65–60}$). There are only three data points between Fo_{60} and Fo_{20} and none between Fo_{34} and Fo_{21}, consistent with the disappearance of olivine from the phenocryst assemblage in the benmoreites. Core compositions in the trachytes range from $Fo_{21·0–17·9}$ in SMN179 to $Fo_{<1}$ in SMN168. MnO and CaO concentrations reach 2·71 and 0·57 wt%, respectively, and generally show negative correlations with mg-number. Concentrations of NiO are very low (≤0·11 wt%), even in the most magnesian rocks.

In Fig. 11, we assess whether the phenocrysts were in equilibrium with their respective whole-rock compositions, using the technique of Reubi & Nicholls (2005).

The distribution coefficients ($^{Fe/Mg}K_{Dmin/liq}$) used were: basalt 0·25–34; mugearite–benmoreite 0·29–0·40; and trachyte/rhyolite 0·40–0·69; and it was assumed that $Fe^{2+} = 0·9\ Fe_{total}$ in the melt. Olivines in the basalts and trachytes have compositions close to equilibrium compositions; cores of ~Fo_{81} in SMN103 and BB85.42 (zoned to a rim of Fo_{57}) probably represent relicts from a higher-temperature stage of evolution. In the mixed rocks, the phenocrysts have clearly been derived from one or more of the mix components.

Clinopyroxene

The compositional range of phenocryst cores is fairly continuous from augite through ferroaugite to ferrohedenbergite ($En_{50–0}$), although there are relatively few analyses

Table 4: Representative analyses of olivine phenocrysts in Olkaria rocks

Strat. unit:	Olkaria Trach. F.		Lolonito Basalt F.		Ndabibi Basalt F.			Magmatic inclusion			
Sample	SMN179		SMN103		BL225a		BL73	BB85.278			
Group:	1		2		1		1	1			
Crystal no.:	1	8	13	13	6	6	1	4	4	5	5
	core	core	core →	→ rim	core →	→ rim	core	core →	→ rim	core →	→ rim
SiO_2	31·81	30·99	38·38	37·74	38·65	36·97	40·16	33·55	35·18	36·69	32·85
TiO_2	0·07	0·06	0·05	0·07	0·00	0·03	0·00	0·08	0·10	0·08	0·13
Al_2O_3	0·00	0·00	0·05	0·03	0·03	0·03	0·07	0·03	0·01	0·03	0·01
NiO	0·00	0·00	0·06	0·04	0·07	0·08	0·22	0·00	0·00	0·00	0·01
FeO*	57·01	61·67	23·22	26·59	21·68	29·47	11·70	50·09	41·21	32·22	54·78
MnO	2·40	2·67	0·34	0·45	0·34	0·47	0·19	1·36	0·93	0·57	1·06
MgO	7·46	2·94	38·60	35·43	39·39	32·84	47·51	15·89	23·33	30·85	12·19
CaO	0·47	0·57	—	—	0·33	0·34	0·33	0·50	0·47	0·26	0·21
Total	99·22	98·90	100·70	100·35	100·49	100·23	100·18	101·50	101·23	100·70	101·24
Fo%	18·9	7·8	74·8	70·4	76·4	66·5	87·9	36·1	50·2	63·0	28·4

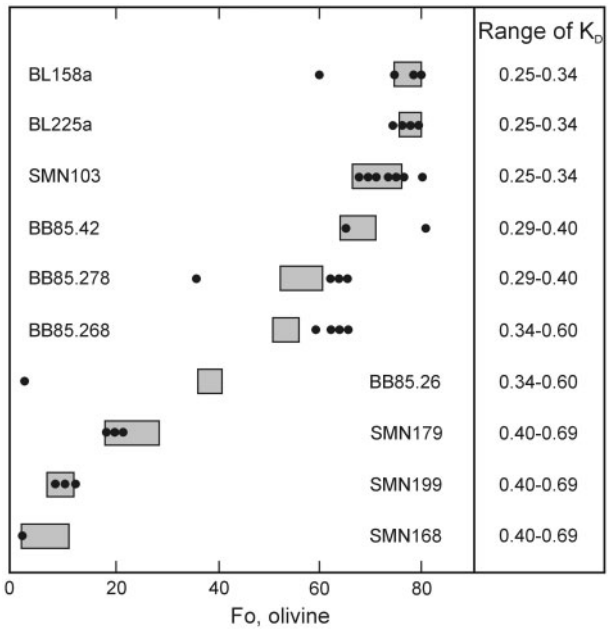

Fig. 11. Composition (in Fo%) of olivine phenocryst cores (•) compared with the compositions of olivines (shaded boxes) calculated to be in equilibrium with melts of the host whole-rock compositions, using the ranges of $^{Fe/Mg}K_{Dol/liq}$ shown. Data from ST3. Based on Reubi & Nicholls (2005).

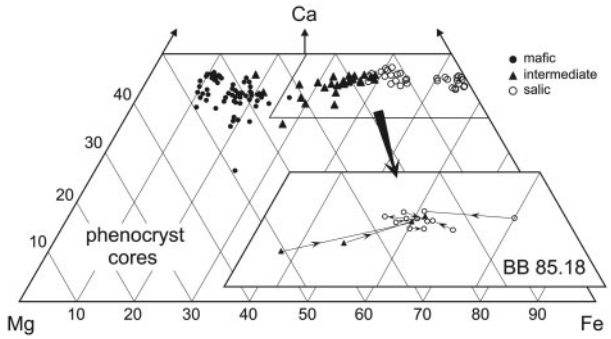

Fig. 12. Composition of clinopyroxene phenocrysts in the Wo–En–Fs triangle. The inset shows zoning relationships in the mixed magma rock BB85.18, with arrows pointing from phenocryst cores to rims. Data from ST4.

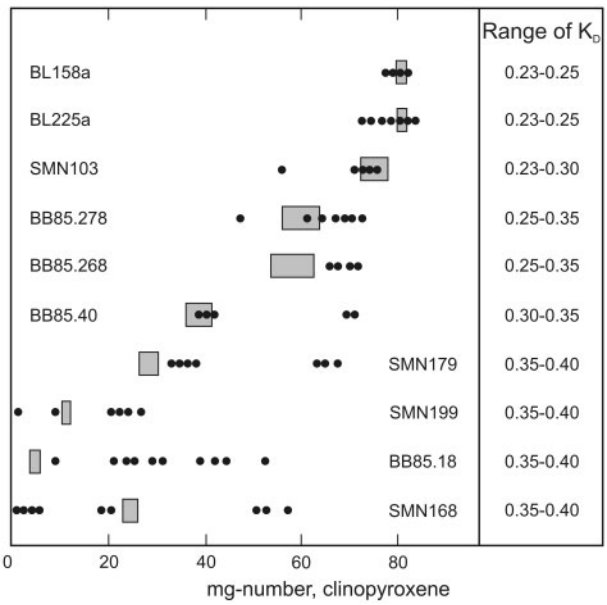

Fig. 13. Composition (as mg-number) of clinopyroxene cores in selected rocks (•) compared with the composition of clinopyroxenes (shaded boxes) calculated to be in equilibrium with melts of the whole-rock compositions, using the range of $^{Fe/Mg}K_{Dcpx/liq}$ shown. Data from ST4. Based on Reubi & Nicholls (2005).

around En_{30} (Fig. 12; Table 5; ST4). Concentrations of Ti and Al are moderate and the two elements show a strong positive correlation. Maximum abundance levels (Ti ~0·1 and Al ~0·33 a.p.f.u., respectively) occur in pyroxenes with mg-number ~55. Sodium abundances are low, even in the most Fe-rich pyroxenes (<0·15 a.p.f.u. = ~5% acmite molecule).

In Fig. 13, we assess whether the phenocrysts were in equilibrium with their respective whole-rock compositions, using the technique of Reubi & Nicholls (2005).

As for the olivines, phenocrysts in the mafic rocks, with core compositions in the range $En_{50–40}$, approach equilibrium compositions. The mixed rocks and trachytes usually contain two or more phenocryst populations, the variable sense of zoning strongly suggesting that the clinopyroxenes from two mixing magmas were attempting to re-equilibrate with the new host composition (Fig. 12, inset).

FeTi-oxides

FeTi-oxides join the phenocryst assemblage in the benmoreites and occur as discrete crystals up to 1 mm long and as inclusions in fayalite, clinopyroxene and alkali feldspar. Both rhombohedral and spinel phases occur mainly as subhedral to heavily resorbed tabular grains, although the rhombohedral phase also forms rods and prisms. Ilmenite occasionally forms thin plates within spinels. Spinels sometimes show exsolution features and both phases can contain sulphide inclusions.

The rhombohedral phase is ilmenite (X_{ilm} 0·97–0·91; Table 6; ST5). Magnesium contents can be moderately high (≤0·09 a.p.f.u.) but Mn contents are invariably low (≤0·03 a.p.f.u.). Niobium abundances range up to 0·02 a.p.f.u. and are variable in crystals in the same rock (e.g. 0·003–0·009 a.p.f.u. in SMN179). No compositional parameter varies systematically with whole-rock composition.

The spinels are compositionally more variable than the ilmenites (X_{usp} 0·55–0·74; Table 6; ST5). Niobium

Table 5: Representative analyses of clinopyroxene phenocrysts in Olkaria rocks

Strat.:	Ndabibi B.F.		Lolonito B.F.		Magm. inclus.		Tandamara T.F.		Olkaria T.F.		Olkaria C.F.	
Sample:	BL229		SMN103		BB85.40		BB85.18		SMN180		SMN168	
Group:	2		2		1		1		1		1	
MC:	1		1		hybrid		hybrid		hybrid		1	
	core	rim	core	rim	core	core	core	rim	core	rim	core	core
SiO_2	52·30	51·19	51·43	49·62	51·41	49·81	50·92	49·36	49·58	48·85	51·31	48·36
TiO_2	0·56	0·85	0·33	1·21	0·99	0·81	0·59	0·58	0·65	0·75	0·48	0·51
Al_2O_3	2·54	3·61	1·44	3·39	1·77	1·19	1·77	1·00	0·95	1·04	1·61	0·24
Cr_2O_3	—	—	0·00	0·00	—	—	0·00	0·00	0·02	0·01	0·01	—
FeO*	5·88	6·93	15·87	10·74	12·06	18·53	16·41	22·43	21·33	22·92	16·26	29·60
NiO	0·03	0·00	0·01	0·00	0·03	0·00	0·01	0·02	0·00	0·01	0·01	0·00
MnO	0·14	0·17	0·61	0·29	0·44	0·76	0·75	0·82	0·76	0·82	0·52	0·96
MgO	16·29	15·69	11·03	15·08	15·00	7·42	9·90	4·91	6·00	4·85	11·85	0·32
CaO	21·70	21·10	19·40	18·69	17·42	20·43	18·50	19·24	19·89	19·78	16·14	19·43
Na_2O	0·26	0·28	0·34	0·36	0·25	0·31	0·42	0·47	0·31	0·34	0·85	0·55
Total	99·70	99·82	100·46	99·38	99·37	99·26	99·27	98·83	99·49	99·37	99·04	99·97
Wo	44·3	43·6	41·2	38·9	36·5	45·2	40·9	44·2	44·3	44·5	35·6	45·2
En	46·3	45·2	32·6	43·7	43·8	22·8	30·6	15·7	18·6	15·2	36·4	1·1
Fs	9·4	11·2	26·3	17·4	19·7	32·0	28·5	40·2	37·1	40·3	28·0	53·7

B.F., Basalt Formation; T.F., Trachyte Formation; C.F., Comendite Formation; Magm. inclus., magmatic inclusion; MC, mix component (see Appendix); —, not determined.

concentrations are low (Nb <0·005 p.f.u.) but Al abundances reach 0·12 a.p.f.u. and Mg contents 0·1 a.p.f.u.

Apatite and chevkinite

We will report on the GOVC apatites elsewhere. Here we note that the major coupled substitution is $REE^{3+} + Si^{4+} = Ca^{2+} + P^{5+}$ and that there is significant solid substitution towards britholite-(Ce). The maximum britholite component, in apatites from SMN168, is 20%. The most REE-rich phases occur in the most evolved rocks (e.g. SMN168 and SMN199).

Chevkinite-(Ce) has been analysed in two trachytes and the salic component of the mixed magma rocks SMN168 and SMN105 (ST6). They conform closely to the general formula for the group; namely, $A_4BC_2D_2Si_4O_{22}$, where $A = (La, Ce, Ca, Sr, Th)$, $B = Fe^{2+}$, $C = (Fe^{2+}, Fe^{3+}, Ti, Al, Nb, Zr)$ and $D = Ti$. There is some variation in the proportions of Ce, La and Ca in the *A* site, although all are chevkinite-(Ce), and of Fe, Ti and Nb in the *C* site. Thus, Ce/La varies from 1·52 to 1·86 and is positively correlated with Fe/Ti, which ranges from 0·58 to 1·74. There is variable LREE enrichment relative to the MREE and HREE; La/Sm and La/Y range from 19 to 56 and La/Y from 10 to 63; both ratios tend to be higher in the chevkinites with lower Ce/La and Fe/Ti ratios.

GEOTHERMOBAROMETRY

Coexisting FeTi-oxides are common in the trachyte lavas (e.g. SMN179, SMN199, BB85.18) and in the salic components of mixed rocks (e.g. BB85.268, SMN168, BB85.40, SMN105). We have analytical data (Table 6; ST5) for three oxide pairs from trachytes; crystal sizes range from 100 to 700 μm and crystals have sharp contacts against glass. None of the pairs is in mutual contact but those in BB85-18 are attached to the same olivine crystal. All three pairs pass the Bacon & Hirschmann (1988) Mg/Mn partitioning test for equilibrium. Temperatures and log fO_2 values calculated using the Andersen & Lindsley (1985) thermobarometer within the ILMAT program of Lepage (2003) are 957°C and −12·35 for SMN199, 950°C and −12·28 for SMN179, and 914°C and −13·48 for BB85.18; these values place crystallization conditions on, or close to, the fayalite–magnetite–quartz (FMQ) buffer. The only other data for trachytes from the CKPP are for pantelleritic trachytes from the Eburru complex (Fig. 1), where Ren *et al.* (2006) used the QUILF thermobarometer to determine temperatures in the range 793–703°C and $fO_2 = \Delta FMQ + 0·5$ to −1·6. The higher temperatures for the Olkaria rocks may reflect their less peralkaline nature, lower volatile contents or reheating of the magmas by more mafic material. The latter process would

Table 6: Average analyses of FeTi-oxide phenocrysts in Olkaria rocks

	Ilmenite					Titanomagnetite					
Strat.:	Mag. inc.	TTF	OTF	OTF	OCF	Mag.inc.	OTF	OTF	OTF	TTF	OCF
Sample:	BB	BB	SMN	SMN	SMN	BB	SMN	SMN	SMN	BB	BB
	85.40	85.18	199	179	168	85.278	199	179	180	85.18	85.268
Group:	1	1	1	1	1	1	1	1	1	1	1
MC:	hyb	hyb	–	hyb	1	hyb	–	hyb	hyb	hyb	1
n:	2	3	5	4	3	5	7	5	5	6	2
SiO_2	0·00	0·00	0·00	0·00	0·00	0·02	0·02	0·02	0·02	0·04	0·05
TiO_2	49·72	49·42	48·40	48·58	49·29	20·48	24·37	23·30	24·82	25·16	22·95
Al_2O_3	0·13	0·09	0·08	0·15	0·05	2·38	0·89	1·09	0·98	0·89	2·06
FeO*	45·91	46·55	46·99	46·95	45·90	72·53	71·03	71·85	70·75	69·51	70·32
MnO	1·06	1·48	1·40	1·35	1·25	0·67	1·19	1·18	1·25	1·25	0·76
NiO	0·00	0·00	0·01	0·00	0·00	0·00	0·00	0·01	0·00	0·00	0·02
MgO	1·75	0·50	0·39	0·91	0·52	1·48	0·29	0·66	0·36	0·39	1·05
Nb_2O_5	0·40	0·80	0·94	0·42	0·94	0·00	0·14	0·06	0·04	0·12	0·01
ZrO_2	0·02	0·13	0·10	0·09	0·01	0·00	0·02	0·03	0·01	0·05	0·03
Sum	98·99	98·97	98·31	98·45	97·96	97·56	97·95	98·20	98·23	97·41	97·25
Fe_2O_3	6·0	5·0	6·2	6·9	4·1	27·6	20·9	23·3	20·2	18·9	22·3
FeO	40·5	42·0	41·4	40·7	42·2	47·7	52·2	50·9	52·6	52·6	50·2
Total	99·6	99·4	98·9	99·1	98·4	100·3	100·0	100·6	100·3	99·4	99·4
ilm	94·2	95·0	94·0	93·2	95·8	—	—	—	—	—	
mt	—	—	—	—	—	59·2	69·2	65·9	70·4	71·9	66·7

Mag. inc., magmatic inclusion; TTF, Tandamara Trachyte Formation; OTF, Olkaria Trachyte Formation; OCF, Olkaria Comendite Formation; MC, mix component (see Appendix); hyb, hybrid rock. Fe_2O_3 and FeO contents determined from stoichiometry using the Ilmat program (Lepage, 2003).

be consistent with the strongly resorbed nature of the alkali feldspar phenocrysts in the trachytes. There would probably be no time constraints on the oxides recording the temperature increase; Pichavant *et al.* (2007) calculated that magnetite should re-equilibrate over distances of the order of 10 μm after 100 days at 900°C.

GEOCHEMISTRY

Group 1

With the proviso that in many cases the terms refer to the bulk composition of mixed magma rocks, the main suite rocks (Group 1) vary from basalts through hawaiites, mugearites, benmoreites and trachytes to rhyolites in the TAS classification scheme (Fig. 14; Le Bas *et al.*, 1986). CIPW norms were calculated using the iron oxidation ratios recommended by Middlemost (1989). The basalts are close to silica-saturation (ne ≤2; hy ≤11); all the more evolved rocks are *hy* ± *q*-normative. The trachytes are mainly metaluminous, although five samples are mildly peralkaline. We have been unable to discern any systematic

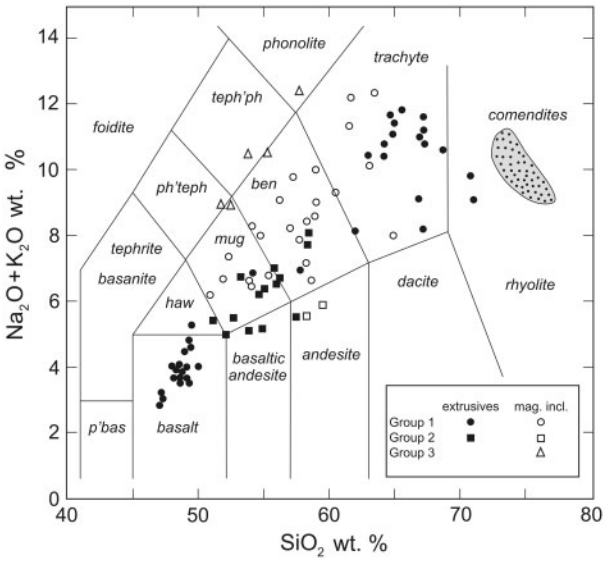

Fig. 14. TAS classification of GOVC rocks (Le Bas *et al.*, 1986). Groups 1, 2 and 3 shown. 'Extrusives' used to include high-level dykes and plugs, and bombs and blocks in pyroclastic deposits. Data from ST7. Data for GOVC comendite field from Macdonald *et al.* (1987).

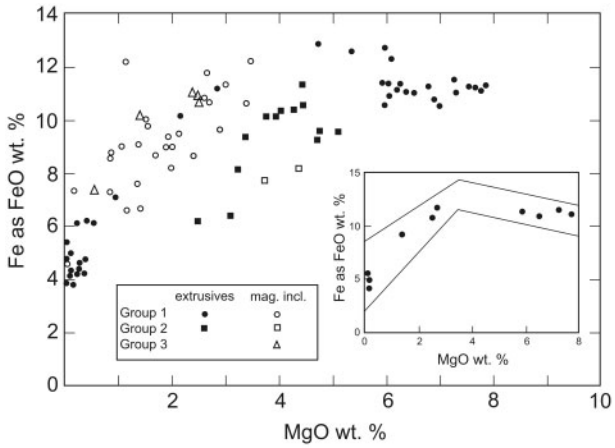

Fig. 15. MgO plotted against FeO* (total Fe as FeO) for GOVC rocks. 'Extrusives' used to include high-level dykes and plugs, and bombs and blocks in pyroclastic deposits. The field in the inset incorporates the Group 1 rocks in the main diagram. The data points in the inset are rocks used to identify the liquid line of descent; namely, BB84.24, BB85.18, BB85.19, BB85.95, BB85.231, BB85.278, BB85.293, BL25, BL30, BL64, BL163, SMN167. Data from ST7.

differences in composition between the mafic rocks of the Lolonito, Ndabibi and Akira Formations; accordingly, they are grouped together in subsequent discussion.

On a MgO–FeO* plot, Group 1 rocks show a peaked trend, with maximum FeO* (total Fe as FeO) abundances of ~13 wt % at 3–4 wt % MgO (Fig. 15). In an attempt to identify the likely liquid line(s) of descent, the inset shows rocks for which there is no petrographic evidence of magma mixing (Appendix) or, with the exception of Ba, significant contamination by feldspar xenocrysts. Group 1 as a whole mirrors the trend shown by these rocks and we infer that the compositional ranges at given MgO values reflect either the presence of several liquid lines of descent and/or additional processes causing scatter.

MgO plots for major elements and selected trace elements are shown in Fig. 16a and b. In each case, the liquid line of descent, as defined above, is also shown. Overall, there are, with decreasing MgO abundance, increases in SiO_2, Na_2O, K_2O, Ga, Rb, Nb, Ta, LREE, Mo, Sn, Zr, Hf and Th, and decreases in CaO, Ni, Cr, Co, V and Sc. Abundances of FeO*, TiO_2, P_2O_5, Li and Sb peak at ~3–4 wt % MgO, and of Ba, Cs and Y at 1–2 wt % MgO. For many elements, there is significant scatter between 3 and 1 wt % MgO. Incompatible trace element (ITE) ratios (e.g. Zr/Nb, Zr/Y, Ce/Y, Ce/Zr, Rb/Zr and Th/U) tend to be constant in the range basalt–benmoreite and then to show much greater ranges in the trachytes.

Part of the scatter at low MgO values is due to the fact at these low abundances, MgO is not an efficient index of differentiation. Using, as an alternative, the Thornton–Tuttle Differentiation Index (DI), there are, with increasing DI, overall increases in SiO_2, Al_2O_3, K_2O, Zr, Nb and the LREE, and decreases in TiO_2, FeO*, MgO, CaO, P_2O_5, Ba, Sr, Y and Na_2O/K_2O (Fig. 17). Zr/Nb, Zr/Y and Ce/Y ratios initially rise gently but then increase more sharply at DI ~85. There are no systematic compositional differences between the Olkaria trachytes, Tandamara trachytes and the trachytic melt inclusions, although the melt inclusions tend to be slightly less evolved (average DI = 79) than the Tandamara trachytes (86) and the Olkaria trachytes (87). The trend includes metaluminous and peralkaline types and we can infer that the trachytic magmas evolved along several lineages close to alumina-undersaturation. Sample SMN118 is anomalous among the trachytes in being *ol*-normative, having low MgO and TiO_2 contents and in being aphyric. It appears to represent a separate lineage.

An important difference in REE distribution between the extrusive rocks and the magmatic inclusions of Group 1 is shown on a Ce–Y plot (Fig. 18). There are two trends in rocks with Ce >100 ppm: with increasing Ce, the majority of extrusive varieties show increasing Ce/Y, whereas the magmatic inclusions show a scattered trend of increasing Y and decreasing Ce/Y. The extrusive trend is essentially that defined by the inferred liquid line of descent and we note below that the Ce enrichment factor along the inferred liquid line of descent (~10) is comparable with that of Zr (~12). Thus rocks with low Ce/Y ratios are Y-enriched, not Ce-depleted. We now explore this further using chondrite-normalized REE patterns.

Davies & Macdonald (1987) presented REE data for 14 rocks from the Ndabibi Basalt Formation. All showed modest LREE enrichment relative to the HREE ($[La/Yb]_{CN}$ 4·8–7·6); 12 samples had positive Eu anomalies (Eu/Eu* 1·03–1·33) and two had Eu negative anomalies (0·70, 0·74). Chondrite-normalized REE patterns for our new data (Table 8) are presented in Fig. 19. Basalt SMN195 shows a smooth pattern with moderate LREE enrichment ($[La/Yb]_{CN} = 7·1$) and a barely significant positive Eu anomaly (1·02). The trachyte lavas are more LREE-enriched ($[La/Yb]_{CN} = 11·2–19·2$) and have variable but large, negative, Eu anomalies ($Eu/Eu^* = 0·59–0·08$).

The patterns in the magmatic inclusions are more diverse (Fig. 19). The rather flat patterns ($[La/Yb]_{CN} = 2·8–8·4$) are a result of strong HREE enrichment (see Fig. 18) and they also show strong negative Eu anomalies (0·55–0·12), the patterns resembling those in the more evolved GOVC comendites (Macdonald *et al.*, 1987). Ytterbium contents reach 62 ppm ($Yb_{CN} = 366$; SMN171), consistent with elevated Y contents (up to 2000 ppm; Tables 7 and 8). We are unaware of such strong HREE enrichment in any magmatic rock. Sample SMN165b is unique in Group 1 in having a positive Eu anomaly ($Eu/Eu^* = 2·0$), whereas two rocks (SMN171 and BB85.40) have significant negative Ce anomalies ($Ce/Ce^* = 0·38$ and 0·33, respectively). Peccerillo *et al.* (2003) reported

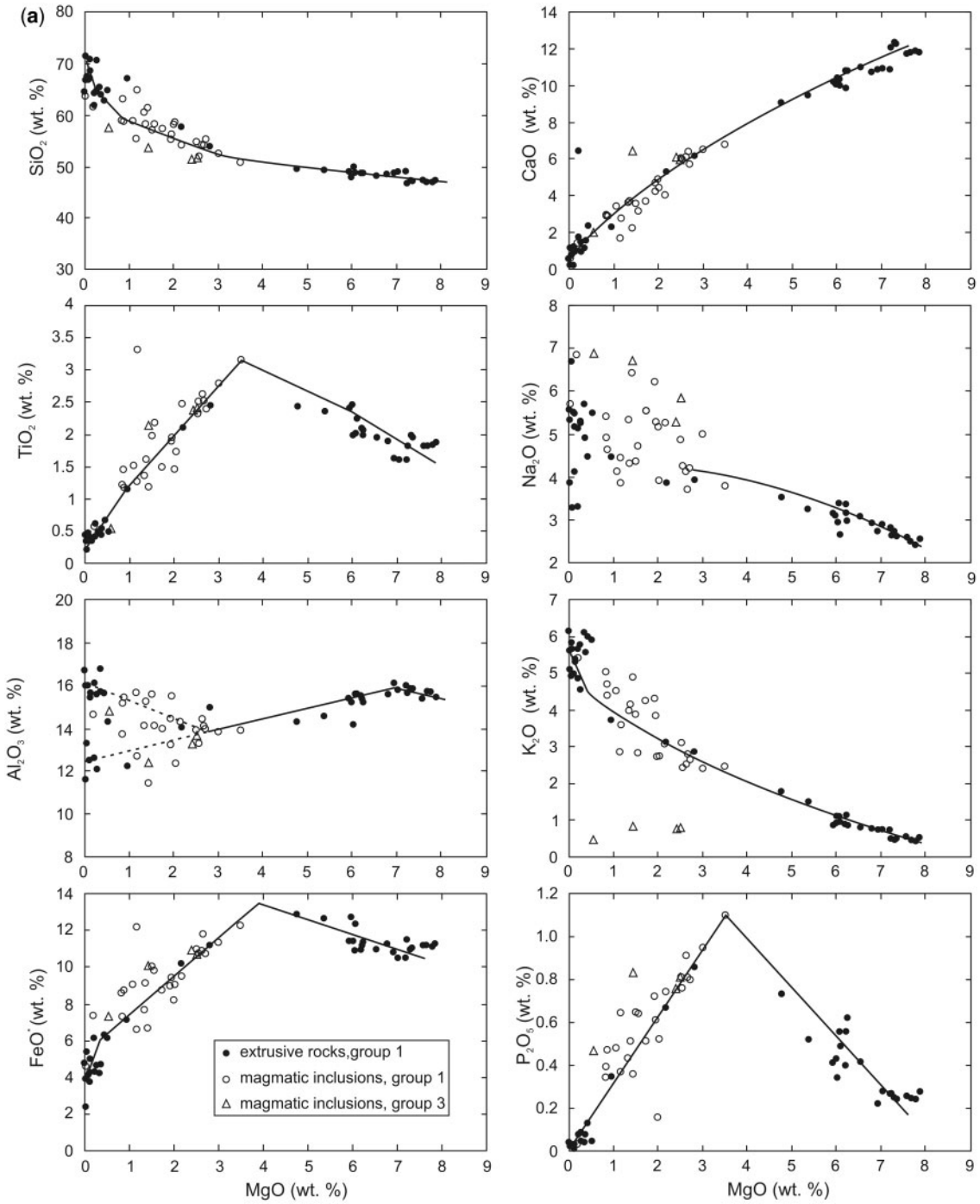

Fig. 16. (a) Whole-rock major element abundances in Groups 1 and 3 rocks (extrusive rocks and magmatic inclusions) as a function of MgO content (wt %). Continuous line is the inferred liquid line of descent (see text for definition). Data from ST7. (b) Whole-rock abundances of selected trace elements in Olkaria eruptive rocks and magmatic inclusions as a function of MgO content (wt %). Continuous line is the inferred liquid line of descent (see text for definition), not shown where element scatter too great. Data from ST7.

anomalous REE enrichment in magmatic inclusions in peralkaline rhyolites from the Gedemsa volcano, central Ethiopian rift, which they related to differential diffusion of these elements from rhyolitic hosts to mafic magmas.

As well as the high abundances in the HREE noted above, some Group 1 rocks show anomalous enrichments in other elements. For example, BB85.01 and BB85.55 have high Zn, Cu and U contents (Zn 3553 and

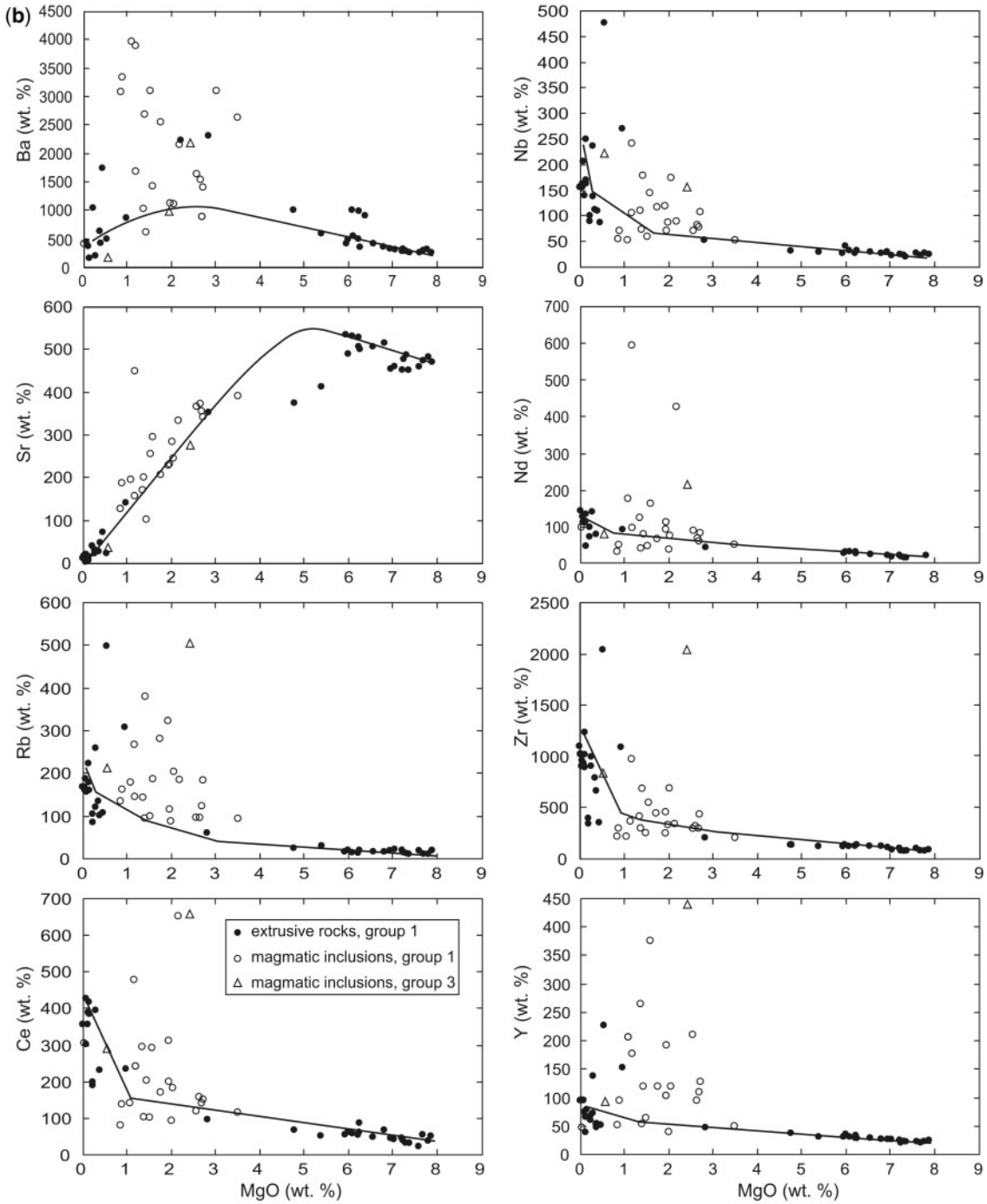

Fig. 16. Continued.

3842 ppm; Cu 225 and 257 ppm; U 60·0 and 62·7 ppm; Table 8), BB85.01 and SMN121 have high Pb contents (233 and 243 ppm, respectively). The high-Y rocks (SMN171, BB85.01 and SMN118) are different from each other; for example, SMN171 has high Fe, Ti, Ba and Sr, whereas BB85.01 has normal abundances of those elements but the high Zn, Cu, U and Pb abundances noted above.

Groups 2 and 3

The location of the Group 2 rocks in the TAS (Fig. 14) and MgO–FeO* plots (Fig. 15), and all other compositional

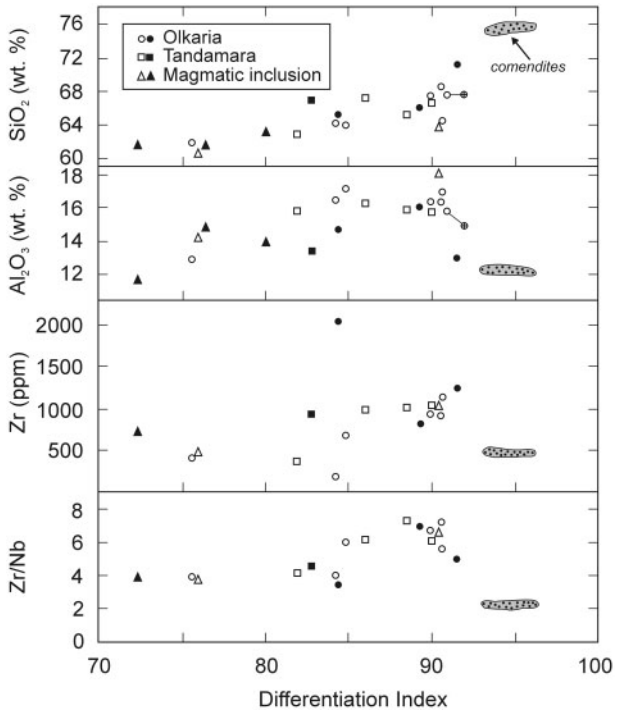

Fig. 17. SiO_2, Al_2O_3, and Zr abundances and Zr/Nb ratio in Olkaria trachytes as a function of Thornton–Tuttle Differentiation Index (q + or + ab). Symbols: circles, Olkaria Trachyte Formation; squares, Tandamara Trachyte Formation; triangles, magmatic inclusions. Filled and open symbols represent *ac*- and *an*-normative varieties, respectively. Shaded field is for the least evolved (Ndabibi centre and Group 1) GOVC comendites (data from Macdonald *et al.*, 1987). Tie-line connects whole-rock and matrix glass compositions in SMN199.

features, are consistent with their being mixtures of mafic and trachytic/rhyolitic magmas, although in many cases the presence of feldspar xenocrysts makes it a three-component calculation. In the straightforward case of the mingled rock BL229, which has neither unusually high Ba contents nor petrographic evidence of feldspar xenocrysts, the end-member proportions are 72% basalt (with 6·5 wt % MgO) and 28% pantellerite (~0·0 wt % MgO). The total range of mafic:salic components is from 85 to 33. Sample BB85.93 has a positive Eu anomaly ($Eu/Eu^* = 1·19$).

Relative to Group 1 rocks of similar MgO content, the *ne*-normative rocks of Group 3 generally have higher abundances of Na_2O and, with the exception of SMN121, high Rb, Th and the REE. Three of the five rocks are peralkaline, with Peralkalinity Indices [PI; mol. $(Na_2O + K_2O)/Al_2O_3$] up to 1·39; the other two (SMN153 and BB85.185) have PI = 0·94 and 0·95 (i.e. are close to peralkaline). Magmatic inclusions SMN153 and SMN169ii show modest LREE enrichment (La_{CN} 624, 717; $[La/Yb]_{CN}$ 9·3, 8·2) and negative Eu anomalies (Eu/Eu^* 0·54, 0·39). SMN121, also a magmatic inclusion, is fairly similar (La_{CN} 418; $[La/Yb]_{CN}$ 9·4) but uniquely in our dataset shows a positive Ce anomaly ($Ce/Ce^* = 1·4$).

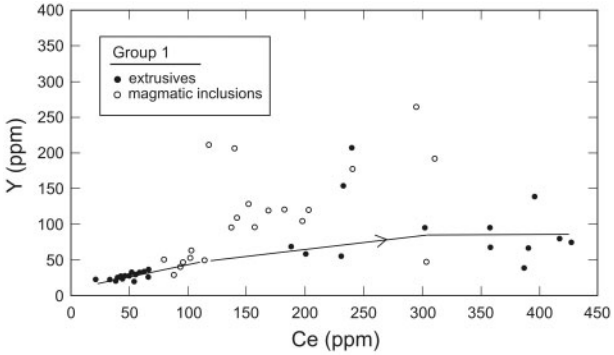

Fig. 18. Ce–Y plot for Group 1 rocks to show the strong Y enrichment in certain magmatic inclusions compared with the majority of extrusive rocks and with the inferred liquid line of descent. Samples BB85.01 (Y = 1119 ppm) and SMN171 (Y = 1892 ppm) are omitted to preserve the scale. Data from ST7.

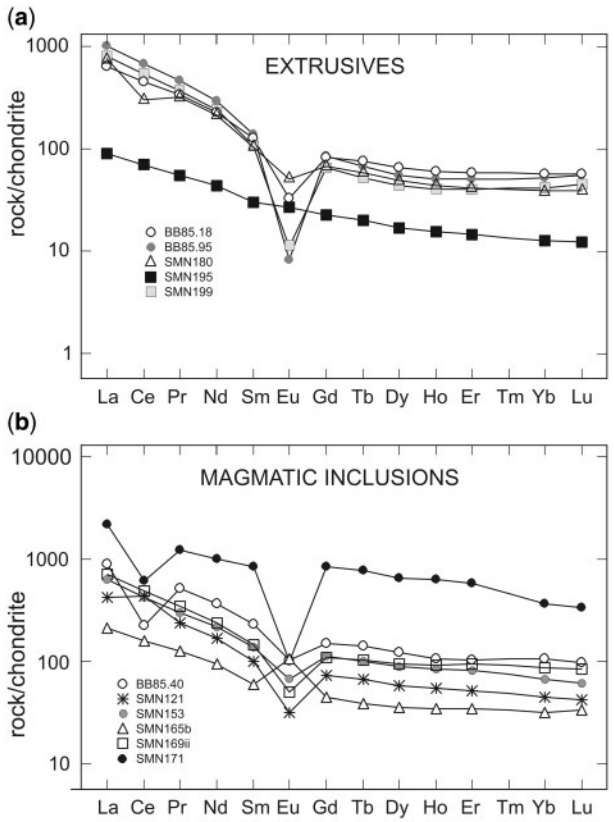

Fig. 19. Chondrite-normalized REE patterns for Olkaria rocks. (a) Extrusives rocks; (b) magmatic inclusions. Data from Table 8. SMN180 and SMN199 are from Olkaria Trachyte Formation; BB85.18 and BB85.95 from Tandamara Trachyte Formation; SMN195 from Ndabibi Basalt Formation. Normalizing factors from Sun & McDonough (1989).

Glass in partially melted xenoliths and feldspars

We have analyses of the glass in partially melted xenoliths and feldspars in SMN103, BL225a and SMN168I

Table 7: Major and trace element analyses (by XRF) of representative Olkaria rocks

Strat.unit:	Olkaria T.F.			Lolonito B.F.		Ndab.	Akira	Tand. T.F.		O.C.F.	Magmatic inclusions													
Sample:	SMN	SMN	SMN	SMN	BB	BL	BB	BB	BB	BL	SMN	BL	BB	SMN	SMN	BB	SMN	BB	BB	SMN	BB	SMN	SMN	BB85.
	179	180	199	195	85.38	225a	85.93	85.18	85.95	563a	158	469	85.231	168.I	153	85.01	169ii	85.25	85.55	171	85.40	165B	121	269N
Group:	1	1	1	1	2	1	2	1	1	2	2	2	1	1	3	1	3	1	1	1	1	1	3	1
SiO_2	63·95	64·11	67·16	49·08	52·06	49·89	55·80	67·26	67·07	58·40	58·15	59·38	50·75	52·30	51·94	54·14	55·26	56·20	58·13	55·19	58·80	58·75	57·73	64·90
TiO_2	0·54	0·61	0·39	1·61	1·97	1·99	1·43	0·45	0·40	1·02	1·12	1·09	3·15	2·79	2·42	2·47	1·99	1·89	2·18	3·31	1·52	1·21	0·53	1·26
Al_2O_3	16·80	16·13	16·05	15·96	14·95	14·14	14·79	13·31	15·62	15·81	14·84	13·83	13·88	13·82	13·71	14·33	13·21	14·43	14·08	15·64	14·46	15·18	14·82	12·71
FeO*	4·64	6·10	4·13	10·50	10·59	11·37	9·61	5·39	4·21	6·19	8·21	7·78	12·25	11·36	10·73	9·52	8·96	9·38	9·81	12·17	9·02	8·58	7·33	6·60
MnO	0·15	0·17	0·12	0·17	0·19	0·21	0·22	0·17	0·11	0·16	0·14	0·13	0·25	0·22	0·19	0·15	0·32	0·22	0·13	0·16	0·16	0·23	0·27	0·12
MgO	0·37	0·21	0·10	7·20	4·43	6·02	3·60	0·06	0·13	2·50	4·39	3·71	3·49	3·00	2·50	2·16	1·93	1·94	1·56	1·16	1·07	0·84	0·54	1·17
CaO	1·52	1·75	1·23	10·86	8·15	10·41	6·44	0·72	1·09	5·77	6·42	5·71	6·78	6·47	5·95	4·05	4·71	4·19	3·13	1·69	3·40	2·92	2·02	2·76
Na_2O	4·91	5·11	5·50	2·82	3·28	2·94	3·79	6·68	5·48	4·43	3·50	3·77	3·78	4·98	5·83	5·26	6·21	5·27	4·73	3·85	4·11	4·90	6·87	4·44
K_2O	5·55	5·65	5·65	0·74	1·71	1·10	2·75	4·90	5·31	3·66	2·06	2·16	2·45	2·40	3·11	3·06	4·30	3·84	2·83	2·85	4·51	5·05	5·52	3·58
P_2O_5	0·08	0·08	0·03	0·27	0·42	0·34	0·37	0·03	0·03	0·20	0·18	0·23	1·10	0·95	0·81	0·74	0·72	0·61	0·64	0·64	0·48	0·39	0·47	0·37
LOI	0·56	0·11	0·13	0·31	0·66	−0·29	0·27	0·26	0·22	0·74	0·65	0·74	0·67	0·55	1·77	2·79	1·14	0·61	1·66	1·36	2·37	0·47	2·55	2·26
Sum	99·07	100·03	100·49	99·52	98·41	98·12	99·07	99·23	99·67	98·88	99·66	98·53	98·55	98·84	98·96	98·67	98·75	98·58	98·88	98·02	99·90	98·52	98·65	100·17
Ba	640	1054	366	280	—	316	1509	51	93	—	1645	263	2630	—	—	2149	987	1116	1419	3883	3962	3073	175	1676
Sr	46	38	12	450	403	383	269	3·6	14	234	293	249	390	—	—	333	228	230	295	449	195	127	36	158
Rb	102	104	158	19	40	32	50	188	159	70	143	143	93	—	—	184	321	117	187	145	179	135	212	266
La	144	199	212	20	71	38	47	177	252	59	62	57	58	—	—	300	190	150	167	702	261	52	109	129
Ce	230	188	357	43	125	70	83	302	417	106	110	125	114	—	—	651	311	198	292	479	140	80	290	240
Nd	79	99	114	21	50	34	38	113	135	42	49	50	52	—	—	426	111	92	164	593	178	33	82	98
Y	54	68	67	25	41	38	39	94	79	40	78	81	50	—	—	1119	191	104	376	1892	206	51	93	177
Zr	662	349	926	105	264	186	198	904	1025	411	478	574	206	—	—	348	457	253	554	367	214	219	841	972
Nb	111	89	139	25	56	48	44	206	171	57	133	151	53	—	—	89	119	71	145	106	54	55	223	241
mg-no.	12·4	5·8	4·1	55·0	42·7	48·6	40·0	1·9	5·2	41·9	48·8	45·9	33·7	32·0	29·3	28·8	27·8	26·9	22·1	14·5	17·5	14·9	11·6	24·0

Olkaria T.F.; Olkaria Trachyte Formation; Lolonito B.F., Lolonito Basalt Formation; Ndab., Ndabibi Basalt Formation; Akira, Akira Basalt Formation; Tand. T.F., Tandamara Trachyte Formation; O.C.F., Olkaria Comendite Formation. LOI, loss on ignition.
*All Fe as FeO.

Table 8: Trace element abundances in selected Olkaria rocks determined by ICP-MS

Strat. unit:	Olkaria T.F.			Lolon.	Ndab.	Akira	Tand. T.F.		O.C.F.	Magmatic inclusions											
Sample:	SMN	SMN	SMN	BB	SMN	BB	BB	BB	SMN	SMN	BL469	SMN	BB	SMN	BB	BB	SMN	BB	SMN	SMN
	179	180	199	85.38	195	85.93	85.18	85.95	168	158	46	153	85.01	169ii	85.25	85.55	171	85.40	165b	121
Group:	1	1	1	2	1	2	1	1	1	2	2	3	1	3	1	1	1	1	1	3
Co	1·8	6·1	1·0	34	48	24	0·2	0·7	3·3	30	28	24	20	16	16	20	19	11	4·8	0·9
Cr	1·0	1·4	0·8	28	51	24	1·3	0·7	285	9·3	49	2·1	1·9	1·9	1·7	1·7	4·9	1·9	1·7	1·3
Ni	0·6	0·4	0·3	23	52	19	0·2	0·2	1328	21	236	3·1	3·4	1·7	1·6	3·8	5·5	1·1	0·4	0·5
Sc	8·3	9·9	5·8	29	36	26	2·7	4·2	3·20	23	21	27	28	20	20	23	24	24	23	2·4
V	3·0	0·8	1·3	232	270	130	0·4	1·0	15·8	179	159	199	200	134	119	172	113	63·4	15·1	1·2
Cu	6·6	7·9	9·9	53	55	28·0	2·8	9·0	11	9·5	13·0	69	225	93	26	257	29	14	17	36
Zn	96	94	91	105	87	101	177	104	196	152	151	860	3553	516	123	3842	427	215	101	277
Ga	24	23	26	22	18	20	31	28	31	24	24	21	25	23	23	24	31	21	21	36
Cs	1·0	0·88	1·6	0·42	0·20	0·61	0·89	1·9	3·7	2·3	1·3	35	6·1	18	6·0	4·6	2·2	23	13	7·5
Hf	15	8·3	17	6·2	2·7	5·2	22	21	24	13	16	8·2	9·2	12	6·7	15	10	5·6	5·70	15
Ta	6·7	5·2	7·8	3·30	1·6	2·80	13	9·6	15	9·2	10	5·2	5·7	7·2	4·3	9·0	6·8	3·4	3·4	12
Li	16	11	18	16	6·6	12	37	28	62	37	43	337	103	182	79	78	43	27	69	139
Mo	3·7	3·1	4·2	1·5	0·73	2·4	3·0	9·1	6·7	3·1	2·8	6·5	3·0	9·3	6·6	3·0	3·6	2·3	3·4	4·2
Sn	5·6	4·4	6·7	2·7	1·3	2·5	11	7·6	15	9·2	9·5	5·8	5·3	11	3·2	5·2	1·7	2·6	3·0	5·5
Sb	0·12	0·12	0·17	0·06	0·03	0·08	0·19	0·21	0·36	0·22	0·18	0·58	0·21	0·52	0·24	0·28	0·27	0·15	0·45	0·67
La	120	177	188	67	21	46	150	234	215	55	51	148	234	170	146	140	509	210	50	99
Ce	207	181	329	125	42	89	277	412	391	99	110	258	559	301	211	266	377	137	97	269
Pr	23	30	35	14	5·2	11	32	43	43	13	13	29	83	33	29	37	115	50	12	22
Nd	74	99	110	51	21	41	106	136	141	46	44	101	368	112	102	153	469	169	45	78
Sm	12	16	16	9·3	4·5	8·0	19	21	25	11	11	21	123	22	18	43	130	35	9·2	16
Eu	1·4	2·9	0·63	2·2	1·5	3·1	1·9	0·48	0·80	1·2	1·1	3·9	6·7	2·9	3·5	4·0	5·8	6·0	6·1	1·9
Gd	10	14	14	8·7	4·6	7·6	17	17	23	11	11	23	156	22	16	54	174	31	9·2	15
Tb	1·6	2·2	1·9	1·3	0·74	1·2	2·8	2·5	3·8	2·0	2·1	3·8	26	3·9	2·4	9·1	29	5·4	1·5	2·5
Dy	9·1	12	11	7·3	4·3	6·8	16	14	22	12	13	22	149	24	14	53	164	31	8·9	15
Ho	1·9	2·5	2·2	1·5	0·87	1·4	3·3	2·8	4·7	2·6	2·8	4·8	30	5·2	2·9	11	35	6·1	2·0	3·1
Er	5·5	6·9	6·6	4·1	2·4	3·9	9·7	8·2	14	7·6	8·3	14	79	16	8·1	29	95	17	5·8	8·6
Yb	5·7	6·6	7·0	3·9	2·1	3·7	9·6	8·8	13	7·4	8·1	11	60	15	7·0	22	62	18	5·5	7·6
Lu	0·88	0·98	1·1	0·58	0·31	0·56	1·4	1·4	2·0	1·0	1·2	1·6	8·3	2·1	1·1	2·9	8·6	2·5	0·84	1·1
Pb	17	8·7	19	5·5	4·5	5·3	21	30	28	21	17	102	233	100	18	79	70	7·7	9·1	243
Th	21	15	29	9·1	2·7	6·8	31	40	45	25	31	39	16	56	14	25	57	8·20	10	17
U	3·8	3·0	5·0	1·4	0·50	1·4	4·8	6·2	9·4	5·1	7·3	9·3	60	11	9·7	63·0	9·9	2·3	4·3	3·1
$[La/Yb]_{CN}$	15·0	19·1	19·2	12·5	7·1	8·9	11·2	19·1	11·9	5·3	4·5	9·3	2·8	8·2	15·0	4·6	5·9	8·4	6·6	9·4
Eu/Eu^*	0·38	0·59	0·13	0·73	1·02	1·19	0·31	0·08	0·10	0·33	0·13	0·54	0·15	0·39	0·63	0·26	0·12	0·55	2·04	0·36

Lolon., Lolonito Basalt Formation; Ndab., Ndabibi Basalt Formation; Akira, Akira Basalt Formation; Tand. T.F., Tandamara Trachyte Formation; O.C.F., Olkaria Comendite Formation; Olkaria T.F., Olkaria Trachyte Formation.

(Table 9; ST7). The glasses cover the range trachyte to rhyolite (SiO_2 62·4–74·6 wt %) and vary from *an* ± *c*- to *ac*-normative. In SMN168I, the deep brown glass is higher in SiO_2, FeO^* and TiO_2 and lower in Al_2O_3, CaO, Na_2O, BaO, *an* and *ab* than the pale brown to colourless glass, whereas K_2O is about constant. All are *an* ± *c*-normative but the PI increases with increasing SiO_2. These trends are consistent with a partial melting sequence in which the earliest melts were enriched in quartz and femic components and later melts increasingly rich in feldspar. Xenolith 3 in BL225a contains both *ac*- and *an*-normative glass, the former types being richer in SiO_2, TiO_2, FeO^*, MnO and CaO, and poorer in Al_2O_3, Na_2O and K_2O, than the latter. This is consistent with an increasing ratio of alkali feldspar to

Table 9: Representative analyses of glasses in partially melted xenoliths

Strat. unit:	Lolonito Basalt F.		Olkaria Com. F.		Ndabibi Basalt Formation					
Sample:	SMN103		SMN168I		BL225a (xen. 1)		BL225a (xen. 2)		BL225a (xen. 3)	
Group:	2		1		1		1		1	
Identifier:	BE	BG	AG	AI	DA	DC	CF	CM	WE	WO
SiO_2	62·66	64·13	66·08	74·22	68·83	74·62	68·28	73·31	69·92	66·10
TiO_2	0·38	0·41	0·00	0·32	0·66	0·54	0·80	0·83	0·30	0·03
Al_2O_3	16·88	17·40	18·23	12·24	12·07	9·70	11·93	12·13	13·07	17·46
FeO^*	3·16	3·22	1·29	2·88	5·60	5·15	6·54	4·96	4·99	1·41
MnO	0·08	0·05	0·02	0·04	0·15	0·14	0·19	0·11	0·16	0·02
MgO	0·42	0·38	0·03	0·02	0·76	0·03	0·02	0·02	0·01	0·03
CaO	2·01	2·38	1·01	0·24	1·56	0·67	0·93	0·50	0·62	0·40
BaO	—	—	0·04	0·01	0·02	0·00	0·00	—	—	—
Na_2O	4·91	4·98	6·36	3·15	4·36	3·64	4·94	2·33	5·04	6·56
K_2O	5·76	5·74	5·43	6·33	4·89	4·72	5·07	4·54	5·28	5·85
Sum	96·26	98·69	98·49	99·45	98·90	99·21	98·70	98·73	99·39	97·86
PI	0·85	0·83	0·90	0·98	1·03	1·14	1·14	0·72	1·07	0·98

PI, peralkalinity index. —, not detected.

mafic components (including sodic pyroxene and/or amphibole) in the residual solids as melting proceeded.

Five glass analyses in xenolith 2 in BL225a are $an + c$-normative and one is *ac*-normative. The only significant compositional difference is in the Na_2O contents ($\leq$2·62 as opposed to 4·94 wt %). Sodium may have been lost from originally peralkaline melts as a volatile (fluoride?) phase. This is consistent with glass data from xenolith 1; the compositional range is very similar to that in xenolith 2 except that Na_2O contents are higher (3·64–4·50 wt %) and the glasses peralkaline. The glasses from SMN103, although trachytic, are less evolved than in the other xenoliths (e.g. SiO_2 62·44–64·13 wt %; $an \geq 5{\cdot}7$). The residual feldspar is also more calcic (An_{32}) and it is likely that this xenolith shows partial melting of a rock more mafic than syenite (syenodiorite?).

Given that peralkaline glasses have been formed by partial melting of the xenoliths, it is instructive to compare their compositions with those of the eruptive comendites of the GOVC. The glasses plot, with the exception of two of pantelleritic composition, in the comendite field on an FeO^*–Al_2O_3 plot (Fig. 20), forming an array parallel to, but displaced above, the eruptive comendites and pantellerites. The glass data from the xenoliths show, therefore, that smaller degrees of melting of syenites inferred to contain sodic pyriboles generated peralkaline rhyolitic melts similar, but not identical, to the GOVC comendites, whereas more advanced degrees of melting, and melting of more mafic xenoliths, generated $an \pm c$-normative trachytes and rhyolites that had no extrusive equivalents.

PETROGENESIS

Causes of the scatter in Group 1

At a given MgO value, the Group 1 rocks show significant ranges of many elements (Fig. 16a and b) and normative characteristics. There were undoubtedly several liquid lines of descent during magma evolution. The variability was extended by basalt–basalt (or hawaiite) mixing in the mafic rocks and mixing between various combinations of mugearite, benmoreite, trachyte and rhyolite in the more evolved rocks. The amount of mixing is difficult to quantify because it caused variations similar to those from crystal–melt processes, although it is usually possible to identify the end-members via the phenocryst assemblages.

Post-eruptive modifications

Peralkaline rocks are prone to compositional modifications on crystallization and/or secondary hydration, particularly loss of Na, oxidation of Fe, and mobility of Rb and Sr. Some Olkaria trachytes are peralkaline and, without analyses of glassy analogues, we cannot preclude the possibility that those rocks lost some Na on post-eruptive crystallization, a possibility also suggested by the fact that some of the *an*-normative trachytes are also mildly *c*-normative (*c.* $\leq$2·5%). Plots of potentially mobile trace elements (e.g. Rb) against immobile elements (e.g. Nb, Zr) for the trachytes are linear, strongly suggesting that the trace elements have not been significantly mobilized during crystallization.

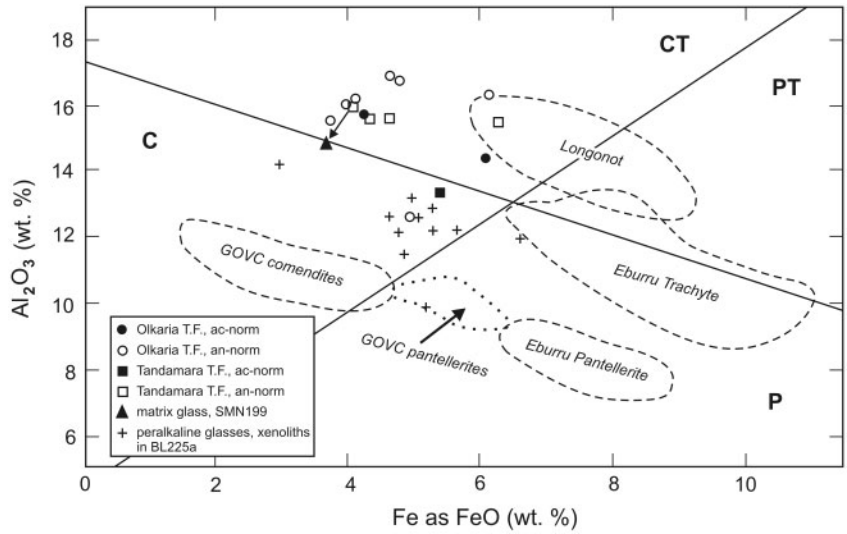

Fig. 20. Fe as FeO vs Al_2O_3 plot for GOVC trachytes (data in ST7) and peralkaline glasses in partially melted xenoliths in sample BL225a (data in ST8). For comparison, the fields of pantellerites and trachytes from the Eburru complex, trachytes from the Longonot volcano, and comendites and pantellerites from the GOVC are shown (from Clarke *et al.*, 1990). Tie-line connects whole-rock and matrix glass compositions in sample SMN199. C, comendites; P, pantellerites; CT, comenditic trachytes, PT, pantelleritic trachytes (fields from Macdonald, 1974).

Feldspar accumulation

The trachytes contain up to 31% alkali feldspar phenocrysts (Table 1) and some rocks may be feldspar-acumulitic. However, there is no correlation in the trachytes between the modal abundance of phenocrysts and the whole-rock Al_2O_3 and FeO* contents, which would be expected to increase and decrease, respectively, as a result of alkali feldspar accumulation. We infer that feldspar accumulation has not been a significant factor in the trachytes and that the high modal proportions reflect large degrees of crystallization in relatively static magmas.

Resorption of feldspar xenocrysts

A large proportion of the Olkaria rocks contain up to ~10% modally of variably resorbed alkali feldspar xenocrysts. Here we assess the compositional effects of the resorption.

Judging from rocks that do not contain feldspar xenocrysts and are not mixed, Ba abundances increase steadily from ~300 ppm in the basalts to a maximum of ~1000 ppm at ~2·5 wt % MgO and then drop sharply to <500 ppm in the trachytes (Fig. 16b). However, 13 samples contain in excess of 2000 ppm Ba. Simple mass-balance calculations show that addition of 3·7 wt % of alkali feldspar with 3 wt % Ba (within the range of values of the Olkaria feldspars; Tables 2 and 3) would increase the Ba content of BB85.23l from 2630 ppm to 4000 ppm, close to the maximum in the suite (Fig. 16b). It is very likely that a significant proportion of the Ba budget of rocks with >1000 ppm has been derived from feldspar resorption, the actual abundances being determined by the amount and composition of the feldspar being resorbed. Anomalous Ba enrichment in alkaline rock suites has previously been ascribed to alkali feldspar resorption by Edgar *et al.* (2002) and Sumner & Wolff (2003). High Ba values can also be used as a guide to the likely former presence of feldspar xenocrysts, now completely resorbed (e.g. in samples SMN171 and BB85.23l). Alkali feldspar resorption also increases the Al_2O_3, Na_2O, K_2O, and usually SiO_2, whole-rock abundances, whereas the content of most other elements is diluted.

Davies & Macdonald (1987) noted that many Ndabibi basalts show positive Eu and Sr anomalies when plotted on primitive mantle-normalized diagrams, which they ascribed to accumulation and/or resorption of plagioclase. Our new data allow us to add some detail. As the An contents of the feldspar phenocrysts and xenocrysts decrease, Eu and Sr abundances initially increase, reaching maxima of ~28 ppm at An_{20} and 1877 ppm at An_{30}, respectively. Abundances of both elements then sharply decrease. As the highest Eu and Sr contents in an Olkaria whole-rock are 6·7 ppm and 550 ppm, respectively (Tables 7 and 8), feldspar resorption has the potential to increase those values. For example, addition of 5% (wt) of feldspar $An_{26·6}$ (analysis 4HC in BB85.40; ST2) to basalt SMN195 (Table 8) increases the Eu abundance from 1·53 to 2·51 ppm. Importantly, the Eu anomaly (Eu/Eu*) increases from 1·02 to 1·73. It is likely, therefore, that positive Eu (and Sr) anomalies in the Olkaria rocks (e.g. Eu/Eu* = 2·04 in SMN165b; Table 8) are a result of the resorption of ternary feldspars in the compositional range $An_{30–20}$. Furthermore, feldspar resorption may have counteracted the development of negative Eu anomalies during fractional crystallization.

Significance of new analyses for the Daly Gap

The eruptive rocks of Group 1, taken to include lavas, high-level dykes, and blocks and bombs in pyroclastic deposits, show an absence of compositions in the range 49·4–62·9 SiO_2 wt % (MgO 4·75–0·52 wt %). This gap is filled by the magmatic inclusions (50·8–64·9 SiO_2 wt %; 4·39–0·03 MgO wt %). The majority of the inclusions are mixed; nevertheless, the compositional range shown by the non-mixed varieties suggests that there was a continuum of melt compositions from basalt to trachyte (Fig. 15, inset). This is consistent with the essentially continuous ranges shown by the cores of feldspar (Fig. 7) and clinopyroxene (Fig. 12) phenocrysts. In addition, the presence of trachytes with $q > 10\%$ and rhyolites in the Olkaria and Tandamara Trachyte Formations provides a transition to the comendites (Fig. 14). Thus the silica-gap between mafic and silicic rocks identified in the GOVC by Davies & Macdonald (1987) and Macdonald *et al.* (1987) does not exist among the magmatic products. A complete spectrum of compositions has existed in the wider plumbing system for the past 20 kyr, although basalts have been erupted largely outside the caldera and mugearites and benmoreites tended to reach the surface only as magmatic inclusions.

A similar situation, where the Daly gap has been filled by magmatic inclusions (enclaves), has been described from the Gedemsa volcano, Ethiopia (Peccerillo *et al.*, 2003), the Alid volcanic centre, Eritrea (Lowenstern *et al.*, 2006) and Pantelleria, Italy (Ferla & Meli, 2006). Bacon & Metz (1984) recorded that intermediate ('andesitic') compositions occur as inclusions in high-silica rhyolites of the Coso volcanic field in California, and Bachmann *et al.* (2002) recorded hybrid andesitic inclusions in the upper intracaldera Fish Canyon Tuff, Colorado. In both the latter cases, the andesites were formed by mixing of basaltic and silicic magmas, as in the GOVC where the majority of inclusions are mixes of two or more components.

Role of fractional crystallization

Major element variations in the Group 1 rocks (Fig. 16a) are qualitatively consistent with fractionation of olivine–clinopyroxene–plagioclase assemblages in the range 8–3·5 wt % MgO, clinopyroxene–plagioclase–FeTi-oxides–apatite from 3·5 to 1·5 wt % MgO, and sanidine–clinopyroxene–FeTi-oxides–apatite ± olivine in the trachytes. We do not present quantitative models of fractional crystallization, because the multi-lineage nature and the complexity of phenocryst or xenocryst relationships (e.g. Figs 7b, 11 and 13) make it virtually impossible to identify likely parent–daughter pairs. Instead, we estimate degrees of crystallization using ITE enrichment factors. The maximum enrichment factor along the inferred liquid line of descent are ~12 for Zr, Rb and Th. Assuming that these elements have been fairly incompatible, the enrichment factors indicate that ~8% of melt (of quartz trachytic to rhyolitic composition) remained after fractionation of parental basalts with 8 wt % MgO, as in the most magnesian members of the Ndabibi Basalt Formation. This value is comparable with those estimated for similar magmatic suites, such as the Gedemsa, Ethiopia, basalt–pantellerite sequence (~10%; Peccerillo *et al.*, 2003) and the basalt–rhyolite suite of the Alid centre, Eritrea (~10–20%; Lowenstern *et al.*, 2006).

Enrichment factors for Ce and Nb are slightly lower at ~10. The fractionation of these elements relative to Zr and Rb occurs in rocks with MgO <3·5 wt % and can probably be ascribed to Ce entry into apatite and chevkinite (ST6) and Nb entry into ilmenite (Table 6). The enrichment factor for Y is ~4 and it has clearly been fractionated relative to the other ITE; we discuss this below.

Relationship of comendites to trachytes

Compositional relationships between the trachytes and the least evolved post-caldera comendites are explored on DI-element/ratio (Fig. 17) and FeO^*–Al_2O_3 (Fig. 20) plots. On the FeO^*–Al_2O_3 diagram, the trachytes plot close to an extension of data for the trachytes from Longonot and Eburru. However, the tie-line from whole-rock to interstitial glass (residual melt) in SMN199 trends towards the comendite field and it is significant that PI increases from 0·94 to 1·01. Thus 26·5% (by volume) crystallization of an alkali feldspar–olivine–clinopyroxene–FeTi-oxide assemblage (SMN199; Table 1) generated a peralkaline residuum. On the DI plots (Fig. 17), the comendites generally lie on extensions of the trachyte field, consistent with a crystal fractionation relationship. The sharp drop in Al_2O_3 and Zr would require fractionation of alkali feldspar and zircon. It is noticeable that the SMN199 tie-line trends towards the comendites for Al_2O_3. Because Zr enters zircon preferentially over Hf, zircon fractionation results in lower Zr/Hf in residual melts (Lowery Claiborne *et al.*, 2006). Trachytes from the Olkaria and Tandamara Trachyte Formations have Zr/Hf in the range 46–50 (Table 8), whereas the least evolved comendites range from 24 to 33 (Macdonald *et al.*, 1987).

The fractional crystallization model for the origin of the comendites resolves a problem raised by the partial melting model (Davies & Macdonald, 1987; Macdonald *et al.*, 1987; Black *et al.*, 1997; Heumann & Davies, 2002). Low Ba–Sr–Eu rhyolites cannot be formed directly by partial melting. Extensive feldspar fractionation from intermediate magma is required, with the formation of cumulates enriched in Ba, Sr and Eu, as we have documented at Olkaria.

The role of accessory mineral fractionation

We noted above that ITE ratios tend to remain about constant in the basalt–benmoreite range but to show greater ranges in the trachytes. Some process, or processes,

fractionated the ratios in the salic magmas. Judging from variations in ITE ratios against DI, the relative degrees of incompatibility were Zr > Ce + Nb > Rb + Th > Y. Rubidium was partitioned into alkali feldspar (Table 3), although the K_D was <1. Y may have been fractionated by apatite; Y_2O_3 levels reach 1·24 wt % in that phase (unpublished data) and there is a positive correlation in the whole-rocks between P_2O_5 and Y. However, apatite fractionation should result in decreased Ce/Y ratios, whereas they increase with increasing DI and there is a negative correlation between P_2O_5 and Ce. Fractionation of LREE-enriched chevkinite would have similar results and chevkinite also concentrates Th (ST6). It seems more likely that Ce (and the other LREE) were partitioned into clinopyroxene, where K_D values of up to three have been recorded from salic rocks (Nash & Crecraft, 1985; Mahood & Stimac, 1990; Sisson, 1991). Either we have not recognized the Y-fractionating phase in the trachytes, or its distribution was not controlled simply by crystal–melt processes, as we suggest below.

Role for a volatile phase?

Certain aspects of GOVC geochemistry may require a role for a volatile phase or phases in magma evolution. We appreciate that the following discussion is speculative but, taken together, the geochemical data point to processes other than simple melt–solid interactions operating in the Olkaria magmas.

(1) Four magmatic inclusions and a trachyte lava have negative Ce anomalies, with Ce/Ce^* in the range 0·91–0·33. Development of negative Ce anomalies is commonly ascribed to oxidation of Ce^{3+} to Ce^{4+} and its being taken up by a halogen-rich oxidizing vapour and lost from the magma. Such a situation is quite probable in the GOVC, where halogen-rich peralkaline magmas were commonly mixing with and/or being heated by more mafic melts, potentially promoting volatile loss. Direct evidence of volatile loss is seen in the vesiculation common at the borders between magmatic inclusions and comenditic hosts. Uniquely in our dataset, magmatic inclusion SMN121 shows a positive Ce anomaly ($Ce/Ce^* = 1·4$). This may be a case of Ce addition through interaction with a volatile phase, a feature consistent with the rock's high Pb content (243 ppm).

(2) Many rocks in the Olkaria suite show anomalous element enrichments; for example, in Y, HREE, U, Cu, Pb and Zn. Yttrium has low solubility in CO_2-rich fluids but, with U, may have partitioned into carbonate melts separating from the silicate magmas. We noted above that the enrichment factor for Y (~4) was much smaller than for the other ITE (≥10). A possible explanation is that Y has been lost from the major parts of the system but concentrated in others. We note that Macdonald *et al.* (1993) documented separation of a carbonate phase from trachytes of the neighbouring Suswa volcano, although no data for Y distribution between the two melts were presented. Enrichment of Pb and Zn may have been via a sulphur-rich fluid phase; sulphide blebs are common inclusions in the FeTi-oxide phenocrysts, indicating that the melts were S-bearing. Lowenstern *et al.* (1991) found that Cu is several hundred times more concentrated in magmatic vapour than in the coexisting melt represented by a pantellerite from Pantelleria and suggested that Cu resides in a vapour phase in some shallow magma chambers, perhaps as CuCl.

(3) Relative to rocks of similar MgO content in Group 1, the *ne*-normative rocks of Group 3 generally have high abundances of Na_2O, Rb, Th and the REE, especially perhaps the HREE (magmatic inclusions SMN153, SMN169ii and SMN121 show only modest LREE enrichment ($[La/Yb]_{CN}$ ~9)). The rocks provide evidence of extensive interaction with the host comendites, including the common growth of fluorite. We suggest that there was selective diffusion into the inclusions of a Na–F-rich fluid, which imparted, *inter alia*, a *ne*-normative, and in some cases peralkaline, character to them.

DISCUSSION

Nature of the Olkaria plumbing system

We have suggested that the following mechanisms operated during the evolution of the Olkaria rocks: (1) crystal fractionation of basaltic magmas generated mugearitic magmas; (2) mixing between basalt magmas was common; (3) further crystal fractionation along several liquid lines of descent produced benmoreitic and trachytic magmas of Groups 1 and 3 and the post-caldera comendites; (4) two- and three-component mixing between mugearites, benmoreites and, less commonly, trachytes produced a range of mingled and hybrid magmas; (5) mixing between basalts and trachytes/rhyolites generated the rocks of Group 2; (6) magma types less evolved than trachytes commonly contain significant amounts of feldspar xenocrysts, presumably derived from the margins of the conduits and reservoirs through which the ascending magmas passed; (7) fluid phases of various composition escaped from, and interacted with, the magmas, possibly a result of heating during mixing; (8) eruption of the comendites was sometimes accompanied by mixing with small amounts of magmas, themselves mixed during an earlier phase.

These features have, to varying degrees, distinguished the GOVC plumbing system since eruption of the oldest Ndabibi basalts (0·5 Ma?) and have affected magmas erupted both inside and peripheral to the ring structure. The system is clearly very open. It is also a very dynamic environment, where crystals with a variety of growth and resorption histories have been juxtaposed shortly before eruption (see Bachmann *et al.*, 2002). The repeated occurrence of different magma types during very short periods

(e.g. the <3 kyr of O^4 activity) strongly suggests that the plumbing system comprises several independent reservoirs and conduits (compare Reubi & Nicholls, 2004, 2005). The reservoirs must be small enough to have been repeatedly pervaded by recharge batches of mafic magma (compare Mammoth Mountain, California; Hildreth, 2004). The concept of the lower parts of the plumbing system being a focus for basaltic dykes is consistent with geophysical evidence. A series of short-wavelength gravity highs (−190 mGal) superimposed on the broad negative anomaly in the axial region of the rift and coincident with the central complexes of the Kenya Dome has been modelled by Swain (1992) as resulting from dyke injection in the central 40 km of the rift. Perhaps 22–26% of the present crust, down to a depth of 22 km, consists of this intruded material.

Magma mixing has been ubiquitous in the development of the GOVC. Indeed, it is uncommon to find rocks in the mugearite–benmoreite range that are not mixed. The swirling textures common between comendites and magmatic inclusions and the intimate admixture of two or three components in some inclusions suggest that significant mixing took place in the conduits. However, the longer times required for hybridization may point to some mixing in small reservoirs. In the basalt–trachyte/rhyolite mixes of Group 2, mingling was more common than hybridization, perhaps pointing either to insufficient time for more complete mixing and/or a viscosity or density barrier preventing mixing. In Group 1 rocks, mugearites and benmoreites have been able to mix with trachytes only where the trachytes have been phenocryst-poor; the crystal-rich eruptive trachytes show relatively little evidence of mingling, although some rocks are hybrids (Appendix). Magmatic inclusions in the comendites show only local interactions with their hosts; more thorough mixing has presumably been prevented by differences in viscosity.

Rejuvenation of earlier mushes and plutonic bodies

Many GOVC rocks in the range basalt–benmoreite, including some erupted outside the ring structure, carry significant amounts of alkali feldspar ± plagioclase xenocrysts. Some also carry gabbro–syenite xenoliths, which have sometimes been partially melted to form silicic melts. The compositions of the xenocrysts are very similar to those of the phenocrysts in the mugearite–trachyte range (Fig. 7a and b) and it seems likely that the bulk of the xenocrysts represent recycled crystals from intrusive rocks or crystal mushes (i.e. are antecrysts). The presence of holocrystalline comagmatic xenoliths indicates that some parts of the plumbing system had crystallized completely. The xenocrysts occur both within and outside the ring structure, possibly indicating that the plutons and mushes were derived from a caldera-scale mass, possibly the residue of the system that generated the syn-caldera rocks.

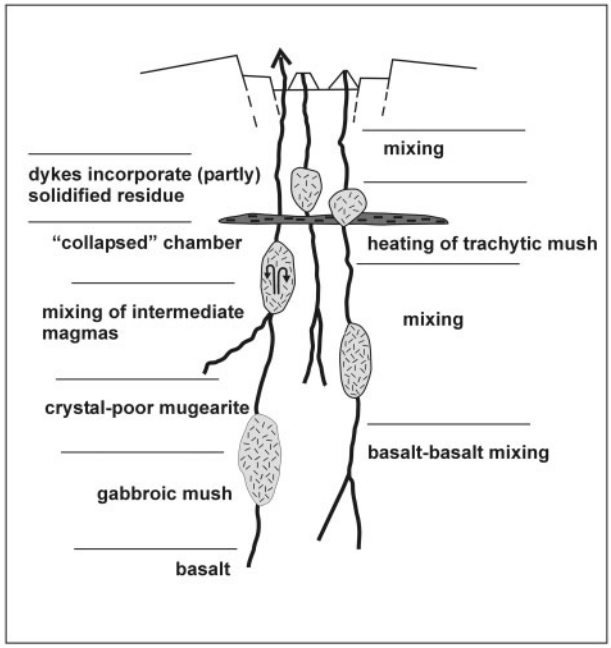

Fig. 21. Schematic illustration of of the GOVC plumbing system. The vertical scale is ~10 km.

No post-caldera pantellerites have been erupted within the ring fracture and it seems possible that the pre-caldera magma reservoir was totally evacuated and that caldera formation resulted in collapse of the roof onto the floor, as envisaged by Macdonald *et al.* (1995) for the basalt–trachyte caldera volcano Silali, in the north–central rift. Later dykes were then able to cut through the former chamber, incorporating xenocrystic and xenolithic material. Material erupted peripherally to the ring structure may have been carried there laterally; there is some evidence in the young volcanoes of the central rift valley of magmas moving between complexes along dykes (Macdonald *et al.*, 1995; Scott & Skilling, 1999; Rogers *et al.*, 2004).

Thermal rejuvenation of near-solidus high-level intrusions shortly before eruption is common in systems of very different volumes (Bachmann *et al.*, 2002) and is probably induced by recurrent pulses of basaltic intrusion and crystallization. Mafic to intermediate magmas may also evolve H_2O–F–S–Cl-rich fluids that flux melting in the crystal mush (Bachmann *et al.*, 2002; the 'gas sparging' effect of Bachmann & Bergantz, 2006) and there is some evidence in the GOVC for the release of such fluids.

Figure 21 is a schematic illustration of the development of the GOVC, based on the various constraints described above. Given the complexity of magma relationships, the scheme is necessarily much simplified and is certainly not definitive. However, the GOVC seems to have similarities to the plumbing system of Batur volcano, Bali, prior to

the second caldera-forming eruption there at ~20 ka, as drawn by Reubi & Nicholls (2005).

The system is driven by basaltic magmas intruded as dykes at mid- to upper-crustal levels. Mingling between basalt magmas sometimes occurs. Basalt ponds at various levels, to form the crystal mushes and/or gabbros recorded as mafic xenoliths in more evolved mixed rocks. Crystal-poor melts of mugearitic–benmoreitic composition are expelled from the reservoirs and rise through dykes, mixing frequently. Incorporation of partially to completely solidified plutonic material is almost ubiquitous during magma ascent. The intermediate magmas pond and fractionate through to trachytes, with crystal residua of syenodioritic composition.

The expelled trachytes pond at ~5–6 km depth, which is comparable with the depth estimated from seismic data to be the interface between the Pan-African basement and the Miocene–Holocene volcaniclastic infill beneath the GOVC (Mooney & Christensen, 1994; Mechie *et al.*, 1997). This may also have been the level at which the pantelleritic magmas erupted during caldera collapse were stored. There is extensive crystallization within the trachytic reservoirs, possibly promoted by gas exsolution, and magma mixing is relatively restricted. The compositional range in the trachytes points to the need for several of these mush-rich reservoirs, which equate, on a smaller scale, with the viscosity barrier of Smith (1979) and mush zone envisaged by Bachmann & Bergantz (2004), Hildreth (2004) and Hildreth & Wilson (2007) for large silicic systems. At a critical value of crystallization, interstitial rhyolitic melts escape upwards as dykes and pods.

Eruption of the rhyolites is either promoted by, or entrains, magmas from deeper levels, ranging from mugearite to trachyte and normally forming two- to four-component mixes. Mafic magmas extruded outside the ring fracture have also incorporated plutonic material and have mixed with rhyolitic magmas.

Origin of the peralkaline rhyolites

Comenditic melts, now represented by glass, have formed by two mechanisms in the GOVC: fractional crystallization of trachyte and partial melting of syenites. The trachytes themselves formed by fractionation of basalts and the inferred liquid line of descent to the least evolved comendites is long, requiring >90% of crystallization. Given the generally phenocryst-poor nature of the comendites, extraction from the parental trachytic mushes must have been very efficient. Extraction would have been aided by the low viscosity of the volatile-rich, peralkaline melts and by gas-driven filter pressing related to volatile saturation and exsolution as crystallization proceded (Sisson & Bacon, 1999; Bachmann & Bergantz, 2004; Simon & Reid, 2005).

Generation of the comendites by partial melting of syenites cannot be excluded on geochemical grounds and the process itself may have been promoted by fluxing of volatiles released from underlying magmas. However, the evidence from the rocks is that partial melting acted on a very small (millimetre) scale and produced a range of rhyolitic compositions, including *an*- and *c*-normative types that have not been erupted as discrete magma bodies. It may well be, however, that at least some of the comendites are mixtures of melts formed by fractional crystallization and partial melting.

CONCLUSIONS

(1) There is a continuum, in the GOVC, of compositions from basalt to comendite, the SiO_2 range 50–63 wt % being represented only by magmatic inclusions.

(2) The trachytes were formed by fractional crystallization of basaltic magmas via mugearites and benmoreites.

(3) Magma mixing has been ubiquitous in all rock types, although hybridization has been less common in the trachytes and rhyolites.

(4) Xenocrystic alkali feldspar occurs in 51% of specimens, up to 9% modally; plagioclase xenocrysts are less common (21%) and less abundant (usually in trace amounts). Some of the xenocrysts have probably been derived through remobilization of partially or completely solidified plutonic material. Xenocryst resorption has had profound effects on certain geochemical features, such as Ba abundances and Eu/Eu*.

(5) The occurrence of peralkaline rhyolitic glasses indicates that the eruptive comendites could have formed by two mechanisms: (a) partial melting of syenites; (b) fractional crystallization of metaluminous trachyte.

(6) Separation of Na- or K-enriched fluids may have generated, *inter alia*, anomalous trace element enrichments in some rocks and a group of silica-undersaturated peralkaline rocks.

(7) The Olkaria system comprises a plexus of dykes, pods and partially to completely solidified intrusions, where ductile deformation promotes extraction, aggregation and mixing of a wide range of melts.

ACKNOWLEDGEMENTS

The Natural Environment Research Council (UK) is thanked for provision of a research studentship to A.S.M. and various research grants to R.M. R.M. gratefully acknowledges tenure of a Visiting Research Fellowship at the Open University during preparation of this paper. Charlie Bacon and John Wolff provided very detailed and helpful journal reviews and Alastair Lumsden for his careful and patient editorial work. We thank Nic Odling (Edinburgh) for help with XRF analyses, and Michelle Higgins and Kay Green (Open University) for the preparation of thin sections. Dr Luc Lepage kindly supplied a copy of the worksheets for his ILMAT program. Field work in Kenya was greatly assisted by Geoffrey Muchemi

and Johnson Mungania at the Olkaria Geothermal Project. The Warden of Hell's Gate National Park and John Mackay and Tim Trent of Oserian Development Co. Ltd made access to parts of the field area possible.

SUPPLEMENTARY DATA

Supplementary data for this paper are available at *Journal of Petrology* online.

REFERENCES

Andersen, D. J. & Lindsley, D. H. (1985). New (and final!) models for the Ti-magnetite/ilmenite geothermometer and oxygen barometer. *EOS Transactions, American Geophysical Union* **66**, 416.

Bachmann, O. & Bergantz, G. W. (2003). Rejuvenation of the Fish canyon magma body: a window into the evolution of large-volume silicic magma systems. *Geology* **31**, 789–792.

Bachmann, O. & Bergantz, G. W. (2004). On the origin of crystal-poor rhyolites: extracted from batholitic crystal mushes. *Journal of Petrology* **45**, 1565–1582.

Bachmann, O. & Bergantz, G. W. (2006). Gas percolation in upper-crustal silicic crystal mushes as a mechanism for upward heat advection and rejuvenation of near-solidus magma bodies. *Journal of Volcanology and Geothermal Research* **149**, 85–102.

Bachmann, O., Dungan, M. A. & Lipman, P. W. (2002). The Fish Canyon magma body, San Juan volcanic field, Colorado: rejuvenation and eruption of an upper-crustal batholith. *Journal of Petrology* **43**, 1469–1503.

Bacon, C. R. & Hirschmann, M. C. (1988). Mg/Mn partitioning as a test for equilibrium between coexisting Fe–Ti oxides. *American Mineralogist* **73**, 57–61.

Bacon, C. R. & Lowenstern, J. B. (2005). Late Pleistocene granodiorite source for recycled zircon and phenocrysts in rhyodacite lava at Crater Lake, Oregon. *Earth and Planetary Science Letters* **233**, 277–293.

Bacon, C. R. & Metz, J. (1984). Magmatic inclusions in rhyolites, contaminated basalts, and compositional zonation beneath the Coso volcanic field, California. *Contributions to Mineralogy and Petrology* **85**, 346–365.

Black, S., Macdonald, R. & Kelly, M. R. (1997). Crustal origin for peralkaline rhyolites from Kenya: evidence from U-series disequilibria and Th-isotopes. *Journal of Petrology* **39**, 995–1008.

Bliss, C. M. (1979). Geology and petrochemistry of the Naivasha area, Kenya Rift Valley. PhD thesis, Lancaster University.

Bone, B. D. (1987). The geological evolution of the S. W. Naivasha volcanic complex, Kenya. PhD thesis, Lancaster University.

Burt, R. M., Brown, S. J. A., Cole, J. W., Shelley, D. & Waight, T. E. (1998). Glass-bearing plutonic fragments from ignimbrites of the Okataina caldera complex, Taupo Volcanic Zone, New Zealand: remnants of a partially molten intrusion associated with preceding eruptions. *Journal of Volcanology and Geothermal Research* **84**, 209–237.

Charlier, B. L. A., Wilson, C. J. N., Lowenstern, J. B., Blake, S., van Calsteren, P. W. & Davidson, J. P. (2005). Magma generation at a large, hyperactive silicic volcano (Taupo, New Zealand) revealed by U–Th and U–Pb systematics in zircons. *Journal of Petrology* **46**, 3–32.

Clarke, M. C., Woodhall, D. G., Allen, D. & Darling, G. (1990). *Geological, volcanological and hydrogeological controls on the occurrence of geothermal activity in the area surrounding Lake Naivasha, Kenya.* Nairobi: Ministry of Energy, 138 p.

Davies, G.R. & Macdonald, R. (1987). Crustal influences in the petrogenesis of the Naivasha basalt–comendite complex: combined trace element and Sr–Nd–Pb isotope constraints. *Journal of Petrology* **28**, 1009–1031.

Edgar, C. J., Wolff, J. A., Nichols, H. J., Cas, R. A. F. & Marti, J. (2002). A complex Quaternary ignimbrite-forming phonolitic eruption: the Poris Member of the Diego Hernández Formation (Tenerife, Canary Islands). *Journal of Volcanology and Geothermal Research* **118**, 99–130.

Feeley, T. C. & Dungan, M. A. (1996). Compositional and dynamic controls on mafic–silicic interactions at continental arc volcanoes: evidence from Cordon El Guadal, Tatara–San Pablo Complex, Chile. *Journal of Petrology* **37**, 1547–1577.

Ferla, P. & Meli, C. (2006). Evidence of magma mixing in the 'Daly Gap' of alkaline suites: a case study from the enclaves of Pantelleria (Italy). *Journal of Petrology* **47**, 1467–1507.

Fitton, J. G., Saunders, A. D., Larsen, L. M., Hardarson, B. S. & Norry, M. J. (1998). Volcanic rocks from the southeast Greenland margin at 63°N: composition, petrogenesis and mantle sources. In: Saunders, A. D., Larsen, H. C. & Wise, S. H. (eds) *Proceedings of the Ocean Drilling Program Scientific Results, 152.* College Station, TX: Ocean Drilling Program, pp. 331–350.

Heumann, A. & Davies, G. R. (2002). U–Th disequilibrium and Rb–Sr age constraints on the magmatic evolution of peralkaline rhyolites from Kenya. *Journal of Petrology* **43**, 557–577.

Hibbard, M. J. (1981). The magma mixing origin of mantled feldspars. *Contributions to Mineralogy and Petrology* **76**, 158–170.

Hildreth, W. (2004). Volcanological perspectives on Long Valley, Mammoth Mountain, and Mono Craters: several contiguous but discrete systems. *Journal of Volcanology and Geothermal Research* **136**, 169–198.

Hildreth, W. & Wilson, C. J. N. (2007). Compositional zoning of the Bishop Tuff. *Journal of Petrology* **48**, 951–999.

Le Bas, M. J., Le Maitre, R. W., Streckeisen, A. & Zanettin, B. (1986). A chemical classification of volcanic rocks based on the total alkali–silica diagram. *Journal of Petrology* **27**, 745–750.

Lepage, L. D. (2003). ILMAT: an Excel program for ilmenite–magnetite geothermometry and geobarometry. *Computers and Geosciences* **29**, 673–678.

Lofgren, G. E. (1974). An experimental study of plagioclase crystal morphology: isothermal crystallization. *American Journal of Science* **274**, 243–273.

Lofgren, G. E. (1980). Experimental studies on the dynamic crystallization of silicate melts. In: Hargraves, R. B. (ed.) *Physics of Magmatic Processes.* Princeton, NJ: Princeton University Press, pp. 487–511.

Lowenstern, J. B., Mahood, G. A., Rivers, M. L. & Sutton, S. R. (1991). Evidence for extreme partitioning of copper into a magmatic vapour phase. *Science* **252**, 1405–1409.

Lowenstern, J. B., Charlier, B. L. A., Clynne, M. A. & Wooden, J. L. (2006). Extreme U–Th disequilibrium in rift-related basalts, rhyolites and granophyric granite and the timescale of rhyolite generation, intrusion and crystallization at Alid volcanic center, Eritrea. *Journal of Petrology* **47**, 2105–2122.

Lowery Claiborne, L., Miller, C. F., Walker, B. A., Wooden, J. L., Mazdab, F. K. & Bea, F. (2006). Tracking magmatic processes through Zr/Hf ratios in rocks and Hf and Ti zoning in zircons: An example from the Spirit Mountain batholith, Nevada. *Mineralogical Magazine* **70**, 517–543.

Macdonald, R. (1974). Nomenclature and petrochemistry of the peralkaline oversaturated extrusive rocks. *Bulletin Volcanologique* **38**, 398–516.

Macdonald, R. & Scaillet, B. (2006). The central Kenya peralkaline province: Insights into the evolution of peralkaline salic magmas. *Lithos* **91**, 59–73.

Macdonald, R., Davies, G. R., Bliss, C. M., Leat, P. T., Bailey, D. K. & Smith, R. L. (1987). Geochemistry of high-silica rhyolites, Naivasha, Kenya rift valley. *Journal of Petrology* **28**, 979–1008.

Macdonald, R., Kjarsgaard, B. A., Skilling, I. P., Davies, G. R., Hamilton, D. L. & Black, S. (1993). Liquid immiscibility between trachyte and carbonate in ash flow tuffs from Kenya. *Contributions to Mineralogy and Petrology* **114**, 276–287.

Macdonald, R., Davies, G. R., Upton, B. G. J., Dunkley, P. N., Smith, M. & Leat, P. T. (1995). Petrogenesis of Silali volcano, Gregory Rift, Kenya. *Journal of the Geological Society, London* **152**, 703–720.

Macdonald, R., Rogers, N. W., Fitton, J. G., Black, S. & Smith, M. (2001). Plume–lithosphere interactions in the generation of basalts of the Kenya Rift, East Africa. *Journal of Petrology* **42**, 877–900.

Mahood, G. A. & Stimac, J. A. (1990). Trace-element partitioning in pantellerites and trachytes. *Geochimica et Cosmochimica Acta* **54**, 2257–2276.

Mechie, J., Keller, G. R., Prodehl, C., Khan, M. A. & Gaciri, S. J. (1997). A model for the structure, composition and evolution of the Kenya rift. *Tectonophysics* **278**, 95–118.

Middlemost, E. A. K. (1989). Iron oxidation ratios, norms and the classification of volcanic rocks. *Chemical Geology* **77**, 19–26.

Mooney, W. D. & Christensen, N. I. (1994). Composition of the crust beneath the Kenya rift. *Tectonophysics* **236**, 391–408.

Nairn, I. A., Shane, P. R., Cole, J. W., Leonard, G. J., Self, S. & Pearson, N. (2004). Rhyolite magma processes of the ~AD 1315 Kaharoa eruption episode, Tarawera volcano, New Zealand. *Journal of Volcanology and Geothermal Research* **131**, 265–294.

Nakada, S., Bacon, C. R. & Gartner, A. E. (1994). Origin of phenocrysts and compositional diversity in pre-Mazama rhyodacite lavas, Crater Lake, Oregon. *Journal of Petrology* **35**, 127–162.

Nash, W. P. & Crecraft, H. R. (1985). Partition coefficients for trace elements in silicic magmas. *Geochimica et Cosmochimica Acta* **49**, 2309–2322.

Peccerillo, A., Barberio, M. R., Yirgu, G., Ayalew, D., Barbieri, M. & Wu, T. W. (2003). Relationships between mafic and peralkaline silicic magmatism in continental rift settings: a petrological, geochemical and isotopic study of the Gedemsa volcano, Central Ethiopian Rift. *Journal of Petrology* **44**, 2003–2032.

Pichavant, M., Costa, F., Burgisser, A., Scaillet, B., Martel, C. & Poussineau, S. (2007). Equilibration scales in silicic to intermediate magmas—implications for experimental studies. *Journal of Petrology* **48**, 1955–1972.

Ren, M., Omenda, P. A., Anthony, E. Y., White, J. C., Macdonald, R. & Bailey, D. K. (2006). Application of the QUILF thermobarometer to the peralkaline trachytes and pantellerites of the Eburru volcanic complex, East African Rift, Kenya. *Lithos* **91**, 109–124.

Reubi, O. & Nicholls, I. A. (2004). Magmatic evolution of Batur volcanic field, Bali, Indonesia: petrological evidence for polybaric fractional crystallization and implications for caldera-forming eruptions. *Journal of Volcanology and Geothermal Research* **138**, 345–369.

Reubi, O. & Nicholls, I. A. (2005). Structure and dynamics of a silicic magmatic system associated with caldera-forming eruptions at Batur volcanic field, Bali, Indonesia. *Journal of Petrology* **46**, 1367–1391.

Rogers, N. W., Evans, P. J., Blake, S., Scott, S. C. & Hawkesworth, C. J. (2004). Rates and timescales of fractional crystallization from ^{238}U–^{230}Th–^{226}Ra disequilibria in trachyte lavas from Longonot volcano, Kenya. *Journal of Petrology* **45**, 1747–1776.

Rogers, N. W., Thomas, L. E., Macdonald, R., Hawkesworth, C. J. & Mokadem, F. (2006). ^{238}U–^{230}Th disequilibrium in recent basalts and dynamic melting beneath the Kenya rift. *Chemical Geology* **234**, 148–168.

Scott, S. C. & Skilling, I. P. (1999). The role of tephrochronology in recognising synchronous caldera-forming events at the Quaternary volcanoes Longonot and Suswa, south Kenya Rift. In: Firth, C. R. & McGuire, W. J. (eds) *Volcanoes in the Quaternary. Geological Society, London, Special Publications* **161**, 47–67.

Simon, J. I. & Reid, M. R. (2005). The pace of rhyolite differentiation and storage in an 'archetypical' silicic magma system, Long Valley, California. *Earth and Planetary Science Letters* **235**, 123–140.

Sisson, T. W. (1991). Pyroxene–high silica rhyolite trace element coefficients measured by ion microprobe. *Geochimica et Cosmochimica Acta* **55**, 1575–1585.

Sisson, T. W. & Bacon, C. R. (1999). Gas-driven filter pressing in magmas. *Geology* **27**, 613–616.

Smith, R. L. (1979). Ash-flow magmatism. In: Chapin, C. E. & Elston, W. E. (eds) *Ash-flow tuffes. Geological Society of America, Special Papers* **180**, 5–27.

Smith, V. C., Shane, P. & Nairn, I. A. (2004). Reactivation of a rhyolitic magma body by new rhyolitic intrusion before the 15·8 ka Rotorua eruptive episode: implications for magma storage in the Okataina Volcanic Centre, New Zealand. *Journal of the Geological Society, London* **161**, 757–772.

Smith, V. C., Shane, P. & Nairn, I. A. (2005). Trends in rhyolite geochemistry, mineralogy, and magma storage during the last 50 kyr at Okataina and Taupo volcanic centres, Taupo Volcanic Zone, New Zealand. *Journal of Volcanology and Geothermal Research* **148**, 372–406.

Sumner, J. M. & Wolff, J. (2003). Petrogenesis of mixed-magma, high-grade, peralkaline ignimbrite 'TL' (Gran Canaria): diverse styles of mixing in a replenished, zoned magma chamber. *Journal of Volcanology and Geothermal Research* **126**, 109–126.

Sun, S.-S. & McDonough, W. F. (1989). Chemical and isotopic systematics of oceanic basalts: implications for mantle composition and processes. In: Saunders, A. D. & Norry, M. J. (eds) *Magmatism in the Ocean Basins. Geological Society, London, Special Publications* **42**, 313–345.

Swain, C. J. (1992). The Kenya rift axial gravity high: a reinterpretation. *Tectonophysics* **204**, 59–70.

Tamura, Y., Yuhara, M., Ishii, T., Irino, N. & Shukuno, H. (2003). Andesites and dacites from Daisen volcano, Japan; partial-to-total remelting of an andesite magma body. *Journal of Petrology* **44**, 2243–2260.

Wolff, J. A. & Gardner, J. N. (1995). Is the Valles Caldera entering a new cycle of activity? *Geology* **23**, 411–414.

APPENDIX: SAMPLE DETAILS

Appendix:

Sample, location, form	Unit	Phenocrysts	Gp:TAS	Xenocrysts	Mix?
Olkaria Trachyte Formation					
SMN177, AJ970963, lava	Ot	af + ol + cpx + ox + ap	1:T	—	—
SMN178, AJ968953, lava	Ot	af + q + cpx + ox + ch	1:=	—	—
SMN179, AJ964948, lava	Ot	af + ol + cpx + ox + ap + z	1:T	—	hyb
SMN180, AJ971965, lava	Ot	af + ol + cpx + ox + ap	1:T	—	hyb
SMN136, AJ972990, lava	Ot	af + ox	1:T	—	—
SMN199, AJ982970, lava	Ot	af + ol + cpx + ox + ap + z + ch	1:T	—	—
SMN198, AJ981973, lava	Ot	=	1:T	=	=
SMN200, AJ978969, lava	Ot	af + q + ol? + cpx + ox	1:T	—	—
BB85.293, AJ992968, lava	Ot	af + q + ol + cpx + ox	1:R	—	—
Lolonito Basalt Formation					
BB85.250, AJ951952, lava	Ba1	1, 2 = ol + cpx + pl	1:B	—	2?
SMN194, AJ957942, lava	Ba1	ol + cpx + pl	1:B	—	—
SMN195, AJ955953, lava	Ba1	ol + cpx + pl	1:B	—	—
BB85.38, AJ998929, lava	Ba1	1 = ol + cpx + pl; 2 = aphyric	2:M	1 = pl	2?
SMN164i, AJ998944, lava	Ba1	1, 2 = cpx + pl + ox	1:M	1, 2 = af + pl	2
SMN103, AJ999931, lava	Ba1	1, 2 = ol + cpx + pl	2:M	1, 2 = pl + af	2
Ndabibi Basalt Formation					
BL30, AK886176, lava	Bn	ol + cpx + pl + ox	1:B	—	—
BL154a, AK886165, lava	Bn	ol + cpx + pl + ox	1:B	—	2
BL218, AK986127, lava	Bn	1, 2 = ol + cpx + pl	1:B	—	2
BL163, AK905175, lava	Bn	ol + cpx + pl	1:B	—	—
BL25, AK904169, lava	Bn?	ol + cpx + pl	1:B	—	—
BL74, AK930154, lava	Bn	ol + cpx + pl	2:BA	af	hyb
BL229, AK928137, lava	Bn	1 = ol + cpx + pl; 2 = ol + cpx + ox	2:BA	—	2
BL146a, AK908172, lava	Bn?	1 = ol + cpx + pl; 2 = aphyric	1:B	—	2
BL158a, AK902170, lava	Bn?	1 = ol + cpx + pl; 2 = aphyric	1:B	—	2
BL64, AK934163, lava	Bt	ol + cpx + pl + ox	1:B	—	—
BL136, AK962179, lava	Bt	1, 2 = ol + cpx + pl	2:H	1, 2 = af	2
BL226a, AK950165, bomb	kBtm	ol + cpx + pl	1:B	af, pl	2
BL124, AK952165, bomb	kBtm	ol + cpx + pl	1:B	af, pl	—
BL223, AK981138, dyke	in kBtm	ol + cpx + pl	1:B	pl + af	2?
BL120c, AK945166, bomb	kBtm	ol + cpx + pl + ox	2:M	af	hyb
BL225a, AK968121, bomb	kBtm	ol + cpx + pl	1:B	af	—
Akira Basalt Formation					
860130, BJ055841, lava	Ba2	ol + cpx + ol	2:M	af	hyb
BB85.42, BJ050851, lava	Ba2	ol + cpx + pl	2:M	af	hyb
BB85.93, AJ992912, scoria	Ba2	cpx + pl	2:M	af	hyb
BB85.94, AJ998818, scoria	Ba2	1 = ol + cpx + pl + ox; 2 = aphyric	2:M	1 = af	2
Tandamara Trachyte Formation					
BB85.18, BJ025863, lava	Tt	ol + cpx + af + ox + ap + z + ch	1:T	—	hyb
BB85.19, BJ028875, lava	Tt	ol + cpx + af + ox + ap + z	1:T	—	—
BB85.95, BJ024874, lava	Tt	ol + cpx + af + ox + ap + z	1:T	—	—
Olkaria Comendite Formation					
BL574, BK033065, block	in Op3	1 = ol + cpx + pl; 2 = aphyric	2:Bn	af, pl	2
BL563a, BK039053, block	in Op3	ol + cpx + pl	2:Bn	af	hyb
SMN168, BJ004940, lava	O4	1 = ol + cpx + af + + q + ox + ap + ch; 2 = aphyric	1:R	—	2

(continued)

Appendix: Continued

Sample, location, form	Unit	Phenocrysts	Gp:TAS	Xenocrysts	Mix?
BB85.268, BJ010978, dyke	?	1 = ol + cpx + pl + af + ox + ap; 2 = aphyric	1:Bn	af	2
SMN105, BJ007980, dyke	cuts O4	1 = cpx + af + q + fl + ap + ch; 2, 3* = ol? + cpx + pl + ox + ap	1:R	af, cpx	3+*
BB84.19, BK019013, plug	O4	=	1:T	=	=
Magmatic inclusions					
SMN158, AK944035, lava	O2	1, 2 = ol + cpx + pl	2:A	af	2
BL469, AK943032, dome	O3	1 = ol + cpx + pl; 2 = af	2:A	af	2+**
BB85.231, BJ011948, plug	O4	ol? + cpx + pl + ox	1:M	—	—
SMN168I, BJ004940, lava	O4	1, 2 = aphyric	1:M	af	2
SMN155, BJ020007, lava	O4	1 = cpx + pl; 2 = aphyric (host)	1:M	af	2
BB84.24, BK019013, plug	O4	aphyric	1:M	—	—
SMN152, BK019013, plug	O4	1 = af + ox; 2 = aphyric	1:M	—	2
BB85.01, BK019013, plug	O4	=	1:Bn	=	=
BB85.54, BK019013, plug	O4	1 = cpx + pl + ox; 2 = af	1:M	—	3 = 2 + 1
BB85.55, BK019013, plug	O4	1 = ol + cpx + pl; 2 = aphyric	1:Bn	—	—
BB85.278, BJ013985, lava	O4	ol + cpx + pl + ox	1:Bn	af, pl, cpx	hyb
SMN153, BJ021009, lava	O4	1 = ol + cpx + pl; 2 = af	3:Pt	1 = af, pl	2
BB85.185, BK018004, lava	O4	1 = ol + cpx + pl; 2 = aphyric	3:Pt	af	3 = 2 + 1
BB85.56, BK020014, aggl	?	1, 2 = ol + cpx + af + ox + ap	1:Bn	—	2
BB85.56P, BK020014, aggl	?	=	1:Bn	=	=
SMN169ii, BJ009944, plug	O4	=	3:Tp	=	=
BB85.25, AJ999932, lava	O4	1 = ol + cpx + pl + ox; 2 = cpx + af + ox + ap	1:Bn	af, pl	2
SMN165ii, AJ998944, lava	O4		1:Bn		
BB85.220, BJ042960, lava		1 = ol + cpx + pl + ox; 2 = aphyric	1:Bn	1 = pl; 2 = af	2
SMN166, AJ998944, lava	O4	1 = cpx + pl; 2 = af + q	1:Bn	af, pl	2
SMN169i, BJ009944, plug	in O4	=	1:T	=	=
BB84.39, BK020007, lava	O4	1, 2 = aphyric	3:Tp	1 = af	2
SMN167, AJ998944, lava	O4	ol + cpx + pl + ox + ap	1:Bn	af	—
SMN80, BJ001912, lava	O4	1 = ol + cpx + ox; 2 = aphyric	1:T	1 = af	2
SMN171, AK956053, lava	O4	1 = aphyric; 2 = af + ox?	1:M	—	2
BB85.269N, BJ010978, dyke	O4	1 = af + q; 2 = cpx + pl + ox; 3 = cpx + pl; 4 = cpx + pl + af	1:T	3 = af; 4 = pl	4
BB85.40, AJ935994, dyke	in O4	ol + cpx + pl + af + ox + ap	1:Bn	af, pl	hyb
SMN165i, AJ998944, lava	O4	—	1:Bn	—	—
BB85.26, AJ999932, lava	O4	1 = ol + cpx + ox; 2 = aphyric	1:T	1, 2 = af	2
SMN165B, AJ998944, lava	O4	cpx + pl + ox	1:Bn	af, pl	hyb
SMN121, BK063052, plug	O4	1 = af; 2 = aphyric	3:P	—	2
SMN118, BK063054, plug	O4	aphyric	1:T	af	—
SMN197ii, AJ972973, lava	O3	—	1:T	—	—
SMN111, BJ011981, dyke	O4	aphyric	=	af	—

Coordinates for locations refer to UTM grid numbers on East Africa 1:50 000 (Y503) topographic maps. Units refer to the stratigraphic subdivisions of Clarke *et al*. (1990). Gp:TAS, Groups 1–3 as defined petrographically and geochemically in the text and classification according to the TAS system (T, trachyte; R, rhyolite; B, basalt; M, mugearite; BA, basaltic andesite; Bn, benmoreite; A, andesite; Pt, phonotephrite; Tp, tephriphonolite; P, phonolite). Mix, the number of components in mingled rocks; hyb, rock believed to be hybridized. —, not present; =, no information; ol, olivine; cpx, clinopyroxene; pl, plagioclase; ox, FeTi-oxides; af, alkali feldspar; ap, apatite; z, zircon; ch, chevkinite; fl, fluorite.
*In SMN105, more than one mafic component.
**BL469 may contain more than 2 mix components.